DEPARTMENT OF PHYSICS,
UNIVERSITY OF JYVÄSKYLÄ
RESEARCH REPORT No. 7/2015

AQUEOUS FOAM AS THE CARRIER PHASE IN THE DEPOSITION OF FIBRE NETWORKS

BY
AHMAD M. AL-QARARAH

Academic Dissertation
for the Degree of
Doctor of Philosophy

To be presented, by permission of the
Faculty of Mathematics and Science
of the University of Jyväskylä,
for public examination in Auditorium FYS1 of the
University of Jyväskylä on November 10th, 2015
at 12 o'clock

UNIVERSITY OF JYVÄSKYLÄ

Jyväskylä, Finland
November 2015

Author: Ahmad Al-Qararah
VTT Technical Research Centre of Finland Ltd
Espoo, Finland
E-mail: ahmad.al-qararah@vtt.fi

Supervisors: Professor Jussi Timonen
Department of Physics
University of Jyväskylä
Finland

Principle Scientist Dr. Jukka Ketoja
VTT Technical Research Centre of Finland Ltd
Espoo, Finland

Senior Scientist Dr. Tuomo Hjelt
VTT Technical Research Centre of Finland Ltd
Espoo, Finland

Reviewers: Professor Jouni Paltakari
Department of Forest Products Technology
Aalto University
Espoo, Finland

Dr. Francisco Garcia-Moreno
Technische Universitat Berlin
Berlin, Germany

Opponent: Professor Stefan Hutzler
School of Physics
Trinity College Dublin
University of Dublin
Dublin, Ireland

ISBN 978-951-39-6320-0 (paper copy)
ISBN 978-951-39-6321-7 (pdf)
ISSN 0075-465X

Abstract

The use of foam, rather than water, as a material carrier in the manufacturing of novel paper-like structures has recently been studied intensively. This new technology provides potential savings in terms of raw materials, energy and water in comparison with traditional water forming. Such foam forming technology can not only produce materials with properties such as improved material homogeneity and reduced density, but also tailor the microporous structures with the foam properties. The pore structures of the foam-formed sheets and water-formed sheets were compared using imaging techniques such as X-ray microtomography, scanning electron microscopy, and light microscopy, which showed that their pore size distributions differed significantly. The relationship of the fibre network and foam properties was investigated by comparing the pore structure with the measured bubble size distribution and it was shown that both the pore structure and corresponding macroscopic sheet properties could be affected by the mean bubble size. The foams were generated with axial mixing, where the bubble size and its distribution was affected by several factors such as rotational speed, air content and surface tension. Responses of wet foam to inclusion of natural and regenerated cellulose fibres were quite different. The mean bubble size became smaller for natural fibres than for regenerated fibres. In addition, the bubble size distribution became narrower for natural fibres. The reason behind this behaviour is likely to be the rough surfaces of the natural fibres and their fine particle fraction, which are absent with regenerated fibres.

Preface

First of all, I would like to express my deepest sense of gratitude to my eminent supervisor at VTT, Dr. Jukka Ketoja, for his patient guidance, encouragement, and excellent advice throughout my study. I was very lucky to have a supervisor like Jukka Ketoja having a genial and courteous personality. He was always ready to give and share his experience with me. For his dedication I express my great appreciation. More gratitude than can be expressed goes to my thesis supervisor, Dr. Tuomo Hjelt, for the fruitful discussions we have had, his advice and support throughout these years. I appreciate all his contributions of time and ideas. He was a great mentor and I sincerely thank him for this. In addition, I would like to thank Professor Ali Harlin for his continuous cooperation in this work and for his great discussions despite his tight schedule. Great thanks also to my thesis supervisor at the University of Jyväskylä, Professor Jussi Timonen, for valuable discussions and excellent guidance. He saw from the start the importance of this work. I would like to thank also the pre-examiners, Professor Jouni Paltakari and Dr. Francisco Garcia-Moreno for their comments in the final phase. Special thanks go to Dr. Christopher Hamlett for his decent comments and proof reading.

I would also like to thank the Technical Research Center of Finland VTT for paving the way for me to accomplish this work. I would like to express my gratitude to my scholarship sponsor, VTT Graduate School. I would also like to extend my thanks for the financial support provided through the EffNet program of Forestcluster Ltd, Academy of Finland (Project “Fibre-laden foams”), European Regional Development Fund (project KOTVA), and Foam Program project.

Special thanks to my office mate Atsushi Tanaka for all the supporting work and for the great time we have had during these years. Great thanks also to Antti Koponen, Harri Kiiskinen, Jani Lehmonen, Karita Kinnunen, Jaakko Asikainen and Erkki Hellén, for fruitful discussions during the course of this work. Special thanks are due to Timo Lappalainen for the great discussion we have had and for sharing his code for the determination of the bubble size distribution. Thank you, Tiina Pöhler, for helpful discussion on pore structure. My thanks are also due to Marie Gestranius and Dilek Ercili-Cura for surface tension measurements, Leila Kostamo, Asko Sneck and Sabine Heinemann for microscopy, Axel Ekman for X-ray

microcomputed tomography. Many thanks also to John Kettle for helpful discussions on mercury intrusion porosimetry.

My time in Finland was made enjoyable in large part due to the great people who I have met during these years. I am grateful for time spent with Idriss, Nurdan, Kirsi, Kalle, Paula, Marja, Tiina, Marah, Vera, Laura, Mehemt, Ahmed and Hakeem. My thanks are also due to my research group members, both old and new – Ari, Jarmo, Martina, Veli-Matti, Elias, Oleg, Cesar, Juha, Sanna, Pasi, Antti, Janne, Johanna, Joonas and Nikolai, for their friendship and for creating a great work atmosphere. Special thanks to Ms. Minttu Haapaniemi for her assistance in getting things done.

My final thanks are due to my family. My biggest and important gratitude goes to my parents who raised me with a love of science and supported me in all my pursuits. Also, my thanks go to my brothers and sisters for their love and encouragement.

Espoo, November 2015

Ahmad Al-Qararah

List of publications

This thesis is based on the following original publications which are referred to in the text as I–IV. The publications are reproduced with kind permissions from the publishers.

I A. M. Al-Qararah, T. Hjelt, A. Koponen, A. Harlin, J. A. Ketoja, Bubble size and air content of wet fibre foams in axial mixing with macro-instabilities, Colloids and Surfaces A: Physicochem. Eng. Aspects 436 (2013) 1130-1139.

II A. M. Al-Qararah, T. Hjelt, A. Koponen, A. Harlin, J. A. Ketoja, Response of wet foam to fibre mixing. Colloids and Surfaces A: Physicochem. Eng. Aspects 467 (2015) 97–106.

III A. M. Al-Qararah, A. Ekman, T. Hjelt, J. A. Ketoja, H. Kiiskinen, A. Koponen, J. Timonen, A unique microstructure of the fibre networks deposited from foam-fibre suspensions. Colloids and Surfaces A: Physicochem. Eng. Aspects 482 (2015) 544–553.

IV A. M. Al-Qararah, A. Ekman, T. Hjelt, H. Kiiskinen, J. Timonen, J. A. Ketoja. Porous structure of fibre networks formed by a foaming process: a comparative study of different characterization techniques. Submitted to Journal of Microscopy.

Paper not included in this thesis

V A. M. Al-Qararah, T. Hjelt, K. Kinnunen, N. Beletski, J. A. Ketoja, Exceptional pore size distribution in foam-formed fiber networks, Nordic Pulp Paper Res. J. 27 (2012) 226-230.

Author’s contributions

Paper I and II: As the first author, I performed the experiments and the data analysis. In addition, I wrote the first draft of the manuscripts.
Paper III: As the first author, I performed the experiments and carried out most of the data analysis. I also contributed in the writing.
Paper IV: As the first author, I performed most of the experiments and the data analysis. I had a major role in writing the manuscript.

Contents

List of abbreviations

CMC	Critical Micelles Concentration
SDS	Sodium Dodecyl Sulphate
MFC	Micro Fibrillated Cellulose
MD	Machine Direction
CD	Cross-machine Direction
2-d	Two-Dimensional
3-d	Three-Dimensional
μCT	Microtomography
SEM	Scanning Electron Microscopy
ESEM	Environmental Scanning Electron Microscopy
LM	Light Microscopy
MIP	Mercury Intrusion Porosimetry
CCD	Charge-Coupled Device
CTMP	Chemi-Thermo-Mechanical Pulp

1. Introduction

> '' Where shall I begin, please your Majesty?'' he asked.
> ''Begin at the beginning,'' the King said, gravely, "and
> go on till you come to the end: then stop."
>
> — Lewis Carroll, Alice's Adventures in Wonderland

The forestry industry is extremely important in Finland. Finland has the vastest forested area in Europe, which covers 75% of the country (Nordic forest owners' association). The paper manufacturing technology is now in decline as for, in particular, printing and writing paper, because news, books, and magazines are also read in electronic devices. Therefore, a need has emerged to develop new fibre based materials combined with reducing the operation costs and at the same time improving the properties of such products. The continuing research of new fibre based products is one of the main functions of VTT Technical Research Centre of Finland Ltd.

In the 1970s experiments were conducted in which foam was used instead of water as the medium in which to suspend the fibres (Radvan and Gatward 1972; Smith et al. 1974; Kidner 1974; Punton 1975). They were able to produce paper-like materials which had a very uniform fibre distribution with increased bulk[1] and porosity. Using this technology, the saving potential is around 30% in raw materials and energy costs (Poranen 2012). The high bulk obtained reduces the raw material use. Furthermore, the forces affecting fibres during dewatering are smaller compared to the conventional water forming. This can save energy during the drying process. However, this forming technology did not find ground in pulp and paper industry at that time.

Foam-forming applications started as a wet-laid nonwoven materials production (Gatward 1973), since foam can handle long fibres. The striking features however of the foam process such as the improved formation and the increased bulk and

1 In the paper industry, the inverted density is often used, which is called the bulk, but there is no qualitative difference between the two.

porosity made this process applicable in the paper making industry. Therefore, considerable interest has been devoted during the last few years to the foam-forming technology at VTT (Poranen, 2012; Lehmonen et al. 2013; Poranen et al. 2013; Lappalainen et al. 2014; Mira et al. 2014). Up-to-date, most of the new fibre based materials have been made in a laboratory scale and only a few in the pilot scale. The development of foam-formed materials is going on with a great interest from industry and researchers.

This dissertation is divided into five chapters. Chapter 1 introduces the motivation and the general objectives of this work. Chapter 2 describes the fundamentals of wet fibre laden foams, in addition to a background regarding the structure and properties of sheets formed by water and foam processes. Chapter 2 also compiles the findings of previous studies on wet fibre laden foams in axial mixing, in addition to the microscopic and macroscopic sheet properties resulting from water- and foam-forming. Chapter 3 describes the experimental set-up and various measurements that were utilized during this study. Furthermore, it also presents a theoretical derivation of the mean radius of the bubble. Chapter 4 pertains to the measurement results and discussion; primarily it is divided into four sections. The first two sections are devoted to the properties of wet fibre laden foams. In the last two parts, a structural comparison between sheets made with foam-forming and water-forming is presented. The last section summarises the work and conclusions are discussed.

1.1 Motivation

As a highly technical attempt, the use of foam in industry as the material carrier instead of water depends profoundly on the accumulation of knowledge. This includes fundamental research in the foam-forming technology. The fundamental research starts with understanding of the properties of wet foams and the interaction of water based foams added with natural and regenerated fibres. Also, studying how fibres affect the properties of pure foams is important. Moreover, the link between the foam properties and the properties of foam-formed samples should be clearer. Furthermore, understanding the relationship between the structure of foam-formed paper and the mechanical and optical properties of such paper is highly important. This work thus contributes to scientific research that aims at improving and promoting the foam forming technology.

This study deals with wet foam, where the typical volume of air in the foam ranges from 60 to 80% and the bubbles are of the order of 20-100 μm in radius. The foam used in this study consists thus of small round bubbles with relatively thick layers of water between them. It is worth mentioning that wet foams have been studied to a lesser extent than dry foams (Exerowa and Kruglyakov 1998).

Foam-forming provides many advantages in comparison with the conventional water-forming. In particular, the formed material has an excellent homogeneity, since fibres inside the foam are mostly trapped between the foam bubbles. This

allows using long fibres and a high consistency[2] stock without significant fibre flocking. As discussed earlier, it is possible to make a very bulky structure using this technology. This feature can reduce the use of raw materials. With foam-forming there is also a possibility to alter the network structure with foam properties. Another thing to note is the suitability of this process to different kind of fibres with different sizes. This opens up a new way to develop tailored materials for a broad range of raw materials.

1.2 Thesis objectives

The aim of the work in this thesis was to understand the formation mechanisms and properties of fibre foams with a view to making novel fibrous paper-like structures. The specific objectives were:

- Study experimentally the foam properties with and without fibres as a function of rotational speed as a result of an axially agitated mixing (Papers I, II).
- To develop a theoretical model for the mean bubble size where the air content is included as a parameter (Paper I).
- Study the response of wet foam to added fibres for a spectrum of fibres of different fibre type and dimensions, and of the properties of the fibre surface (Paper II).
- Study the pore structure of foam-formed sheets. The results were compared with those for similar structures obtained with water-forming (Paper III).
- Study the effect of foam bubble size on the fibre networks formed by a foaming process (Paper III).
- Making comparison between different characterisation techniques to find suitable techniques for assessing the pore structure of low density materials (Paper IV).

[2] The term consistency refers to the mass fraction of solid material in suspension.

2. Background

> "That is part of the beauty of all literature.
> You discover that your longings are
> universal longings, that you are not lonely
> and isolated from anyone. You belong."
>
> — F. Scott Fitzgerald

This chapter presents a brief overview of fibre laden foams and characterisation of the void structure of foam-formed fibre networks. A general introduction to foams, and to properties of surfactants and foams, is given, followed by an overview of fibre laden foams and foam-forming. Pore structure analysis of both foam-formed and water-formed sheets is described in detail. Finally, the strength properties of foam-formed and water-formed sheets are discussed.

2.1 Foam

This section is a review on foam properties, gives a theoretical background to bubble rupture mechanisms and discusses some rheological studies on the foam.

2.1.1 Foam basics

Foam can be defined as a system consisting of dispersed gas bubbles in a liquid matrix (Weaire and Hutzler 1999; Cantat et al. 2013; Exerowa and Kruglyakov 1998). The air percentage inside the foam determines whether the foam is ''dry'' or ''wet''. Dry foam is produced when the air content is higher than 80%, which means that the liquid fraction is limited to a small amount of water in the so called Plateau borders[3] and bubble vertices (Weaire and Hutzler 1999). The shape of the

[3] The edges of polyhedra at which three films meet.

bubbles in this case is not spherical, but they rather have a polyhedral shape. On the other hand, wet foam is produced when the air content in the system is between 60-80%, where the shapes of the bubbles are spherical with quite thick layers of water between bubbles. Figure 2.1 shows examples of both wet and dry foam.

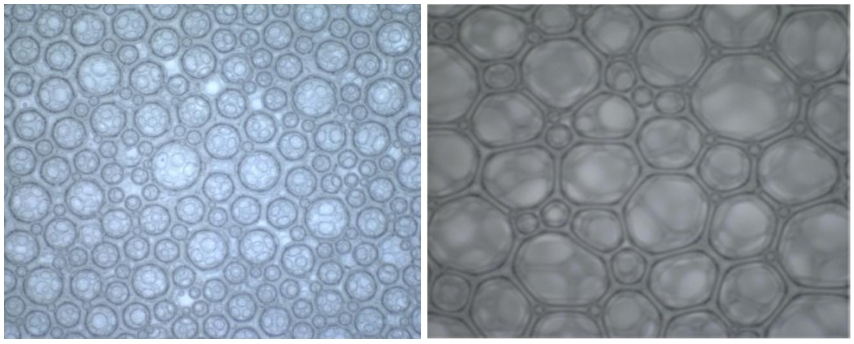

Figure 2.1. Wet (left) and dry (right) foam. The size of the images is 1.8 mm x 1.5 mm.

In order to make foam, a surfactant is needed as pure liquid does not foam (Rosen 2004; Pugh 1996; Malysa and Lunkenheimer 2008). Surfactant molecules absorb at the air-water interfaces such that they alter the free energy of those surfaces (Rosen 2004) and are made up of both hydrophobic and hydrophilic groups. In an aqueous solution when surfactant molecules are dissolved, the hydrophobic part starts to distort the structure of the water (Rosen 2004). As a consequence of that, surfactant molecules move to the interface which becomes covered with a layer of surfactant molecules with their hydrophobic part oriented towards the air. Thus, the surface tension of water is decreased.

At a higher concentration called the critical micelles concentration (CMC), micelles are formed, all additional surfactants go to the micelles, and the surface tension becomes constant.

The surfactants can be classified into four categories according to their hydrophilic group: anionic, cationic, zwitterionic and non-ionic surfactants (Rosen 2004). In this work, the anionic surfactant Sodium Dodecyl Sulphate (SDS) was used. The molecular formula of SDS is shown in Fig. 2.2.

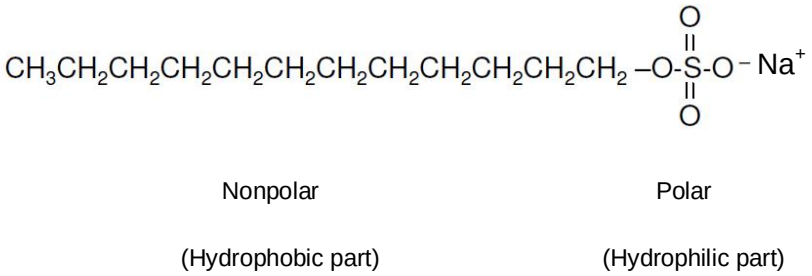

Figure 2.2. Sodium Dodecyl Sulphate (SDS), $C_{12}H_{25}OSO_3^-Na^+$.

SDS is used in many different industrial applications. It is commonly used in e.g. shampoos, toothpastes and shaving creams. The price of SDS is quite low. SDS has a small molecular mass (289.4 g/mol) and thus it diffuses easily. It can therefore be used for a rapid foaming.

The choice of the type of surfactant depends on application requirements. Different kinds of surfactants have been investigated by (Mira et al. 2014) in terms of the rate of foam generation and liquid drainage. An important conclusion was that SDS and two other surfactants allowed a more rapid forming than the others. In a recent thesis (Sievänen 2010), a comparison between casein, polyvinyl alcohol (PVA) and SDS in foam formation has been made. The best results in foam stability were achieved for SDS.

2.1.2 Air content and bubble size distribution

Foam can be produced by using various methods of introducing gas into an aqueous solution of surfactants (Weaire and Hutzler 1999; Cantat et al. 2013; Exerowa and Kruglyakov 1998). The most common method however of foam generation in industry is use of a mechanical mixer and it is surprising how little research has been done on this foam generation method, mainly because of the complex coupling between the macroscopic flows in the vessel and the rheology of the foam.

Important parameters of the foam are air content and bubble size distribution, which play significant roles in determining the structure of the end product since they have an impact on foam properties such as viscosity, stability and drainage. The bubble size distribution was considered to be the most important parameter in determining the end products of the textile substrates, where foam has been used as the material carrier (Isarin 1985). Also, the bubble size distribution has been found to be extremely important in a both ore and wastewater treatment (Rodriques and Rubio 2003).

There have been numerous studies in the last decades conducted on the determination of the bubble size distribution. The experimental techniques used have mainly been the electrical conductivity (Clark 1948; Xie et al. 2004) and direct image processing (Lappalainen and Lehmonen 2012; Ventura and Cilliers 2000).

The air content and bubble size distribution depend however profoundly on the way the foam is generated. For example, if the foam is generated by a mechanical mixer, then the air content and the bubble size distribution can be varied by changing the rotation speed of the mixer (Lappalainen and Lehmonen 2012). It has been found that the bubble size distribution is mainly determined by the shear stress in the mixer (Kroezen and Groot Wassink 1987).

2.1.3 Bubble rupture mechanisms

There are many articles which discuss the bubble formation and their break-up for various foam generation methods (Skelton 1987; Saint-Jalmes 2006; Wang and Neethling 2009; Darton and Sun 1999; Hinze 1955; Nazarzadeh and Sajjadi 2010; Hohler and Cohen-Added 2005). Most of the models proposed are for the air lift system, where the small bubbles are formed in the liquid by blowing air into the system. These models are based on determination of the forces which affect the motion of a single moving bubble in the liquid.

In order to break-up a bubble, it has to be first deformed, and at this stage the Young's-Laplace's equation plays an important role, where the pressure difference between the inside and outside of the bubble can be determined from

$$\Delta P = \sigma \left(\frac{1}{r_1} + \frac{1}{r_2}\right), \tag{2.1}$$

where σ is the surface tension and r_1 and r_2 are the principal radii of curvature. In the case of a spherical bubble of radius r, Eq. (2.1) reduces to $\Delta P = 2\sigma/r$. This equation tells us that the difference in pressure depends on the surface tension and the radius of the bubble. The pressure inside a small bubble is greater than in larger ones. Assuming that r = 15 μm and σ = 63 mN/m, we have a Laplace pressure around 10^4 Pa. Therefore, in order to deform such a bubble, an external stress in excess of this value should be applied. To achieve such high shear stresses, a sufficient energy needs to be introduced into the system. This equation also indicates that the amount of energy needed to deform and break-up the bubble is less when the surface tension is lower, which can be achieved by adding more surfactant. Moreover, the type of flow is extremely important, where eddies of a length scale smaller than the bubble size are required to break the bubble, whereas larger eddies merely transport the bubble (Clift et al. 1978). Depending of the type of the flow, the cause of deformation varies.

The capillary force that resists a shape change can be expressed in the form

$$F_{\text{capillary}} = 2\pi r \sigma \tag{2.2}$$

with r the radius of the bubble and σ its surface tension.

If we consider a single bubble moving slowly in a liquid phase, we can estimate the viscous force acting on it. The drag force of a liquid on a spherical bubble depends linearly on velocity and is given by Stokes' law,

$$F_{drag} = 6\,\pi\,\mu\,u_b\,r, \tag{2.3}$$

where μ is the dynamic viscosity of the suspending liquid, r is the radius of the bubble and u_b is the velocity difference between the bubble and the fluid. This linear dependence holds only at low Reynolds numbers (Re < 1). At higher bubble velocities the drag force becomes

$$F_{drag} = C_D \frac{\pi}{4} d_{max}^2 \frac{1}{2} \rho_l u_b^2, \tag{2.4}$$

where C_D is the drag coefficient, d_{max} is the maximum stable bubble size, and ρ_l is the liquid density. The drag coefficient is a function of Reynolds number. At low Reynolds numbers, the drag force is proportional to u_b instead of u_b^2. Therefore, Eq. (2.4) reduces to Eq. (2.3).

The bubble starts to break-up once the capillary force is smaller than the drag force. Another dimensionless number, the capillary number (Ca), is often used to compare the liquid viscosity and surface tension,

$$\frac{F_{drag}}{F_{capillary}} = \frac{6\,\pi\,\mu\,u_b\,r}{2\,\pi\,\sigma\,r} = \frac{3\,\mu\,u_b}{\sigma} = Ca. \tag{2.5}$$

The other dimensionless number is the Weber number (We) which represents the relative effect of inertial forces and the surface tension,

$$\frac{F_{drag}}{F_{capillary}} = \frac{C_D \frac{\pi}{4} d_{max}^2 \frac{1}{2} \rho_l u_b^2}{2\,\pi\,\sigma\,r} = \frac{C_D\,\rho_l\,r\,u_b^2}{4\,\sigma} = We. \tag{2.6}$$

If the rupturing force acting on a bubble is the shear stress, the force acting on the bubble becomes

$$F_{stress} = \tau\,A = \mu\,\dot{\gamma} A, \tag{2.7}$$

where τ is the shear stress, μ is the viscosity, $\dot{\gamma}$ is the shear rate and A is the cross-sectional area. The capillary number can be expressed in the form

$$Ca = \frac{\mu \dot{\gamma} r}{\sigma}. \tag{2.8}$$

The bubble will start to break-up once the critical values of Ca or We are exceeded. Thus, the estimated bubble radius follows the relations:

$$r_{max} = constant \frac{Ca_{crit}\, \sigma}{\mu \dot{\gamma}}, \tag{2.9}$$

$$r_{max} = constant \frac{We_{crit}\, \sigma}{\rho_l\, u_b^2}. \tag{2.10}$$

Equation (2.9) is used for systems, where viscous shear forces dominate the bubble-fluid interaction, whereas Eq. (2.10) is used for systems, where inertial forces are dominant. Typical values of the critical Weber number are 2-22 for air bubbles in water [Darton and Sun 1999], while the critical capillary number has a value in the range 5-25 for isolated bubbles. The capillary number for foam can be an order of magnitude smaller [Gonzenbach et al. 2007; Denkov et al. 2009; Tcholakova 2008].

Gonzenbach an coworkers (Gonzenbach et al. 2007) used Eq. (2.9) to describe the rupture of bubbles in a wet foam stabilized with partially hydrophobized inorganic particles as a balance between interfacial stresses and shearing stresses applied during the mixing process. The air content in the foam ranged from 45 to 90% and the bubbles were of the order of 10-200 μm in radius. An important conclusion was that the average bubble size decreased according to Eq. (2.9) as both the amphiphile content and particle concentration were increased. They attributed that to a decrease in the surface tension of the suspension and to an increase in the effective foam viscosity.

2.1.4 Viscosity of foams

Foams are non-Newtonian fluids, which means that their viscosity depends on the shear rate. The measured shear stress of a foam is usually fitted using the Herschel-Bulkley equation,

$$\tau = \tau_0 + K\dot{\gamma}^n, \tag{2.11}$$

where τ_0 is the yield stress, n is a flow index and K is a consistency index. The viscosity of the fluid is given by

$$\mu_{eff} = \frac{\tau_0}{\dot{\gamma}} + K\dot{\gamma}^{n-1}. \tag{2.12}$$

At a high shear rate the first term is negligible, and the values for K and n can be found by fitting Eq. (2.12) to the data.

Pipe flow was incorporated in the first published rheological results on fibre laden foams (Jäsberg et al. 2015), in which the slip velocity and bubble size were measured using a high speed imaging technique. The air content of the foam was around 70% and its consistency was 2%. They found the average value $n \approx 0.5$. This value was in agreement with the value predicted by (Tcholakova et al. 2008). Many scientists have however fitted their experimental data on pure foams with the Herschel-Bulkley equation, and reported a flow index in the range 0.25 to 1.0 (Hohler and Cohen-Addad 2005; Gardiner et al. 1999; Larmignat et al. 2008).

2.2 Fibre laden foams

This section discusses the types of fibre used in the experiments described in later chapters and in addition an introduction to foam forming technology is also presented.

2.2.1 Fibre sources

Paper-like materials are made out of cellulose fibres. Fibres can be classified according to their origin as natural or man-made fibres. Natural fibres are found in plants, animals or minerals. The wood fibres are made of cellulose, hemicellulose and lignin. The paper properties are determined based on fibre properties. The fibre properties can vary with the wood species and pulping method (Niskanen 2008). The man-made fibres can be classified into regenerated and synthetic fibres. The regenerated fibres are those made of natural polymers, whereas the synthetic fibres are made of synthetic polymers. Wood is disintegrated into fibres by a process called pulping. There are two different types of pulping, namely chemical and mechanical pulping (Niskanen 2008).

Differences of chemical and mechanical pulps lead to different sheet properties. For instance, the lignin content is as high as 30% after mechanical pulping, but can be negligible after chemical pulping (Niskanen 2008). The fibres can also be damaged during mechanical pulping, and can be associated with a high fines content. The density of sheets made of a mechanical pulp is low and the fibres are stiff. In chemical pulping fibre damage is low in comparison with mechanical pulping and the fibres are more flexible. Paper made up of a chemical pulp is stronger.

2.2.2 Foam forming technology

In the mid 1970s several articles were published using foam in papermaking as a fibre suspending medium instead of water (Radvan and Gatward 1972; Smith et al. 1974; Kidner 1974; Punton 1975). The foam was generated by adding a small amount of surfactant to the pulp and injecting air under controlled conditions, the

air content of the foam was around 65% and the bubble size was 20 to 100 μm in diameter. The fibre consistency was between 0.75 and 1.0%.

In foam forming, wood-pulp is mixed with foam, and this mixture is transferred through the headbox to the wire, where foam is removed using a vacuum. The fibres are essentially separated by foam bubbles until they collapse because of the vacuum. This provides excellent sheet homogeneity, and enables the use of high consistency stock. In addition to that, a high bulk and porosity can be obtained. The main drawback of this technology is a decrease in strength. The loss in strength can be regained by wet pressing and/or beating (Smith et al. 1974).

This area of research has been actively investigated by VTT for the past few years. Most of the recent research on using foam in papermaking at VTT has been aimed at producing material with a very homogeneous distribution of fibres with a very bulky structure and high tensile strength. To address the loss of strength in foam-formed sheets, it has been demonstrated that the strength of foam-formed sheet can be regained by using micro-fibrillated cellulose (MFC) without losing the bulky structure (Kinnunen et al. 2013).

It is highly important however to understand the interaction of foam and fibres, and how fibres affect foam properties. The effects of adding natural fibres to foam under dynamic mixing conditions have been studied, and it has been found that the bubble size has been reduced when natural fibres have been added, because of an increase in the liquid viscosity (Lappalainen and Lehmonen 2012).

2.3 Fibre network structure

Paper is a complex material comprised of a network of bonded fibres. The macroscopic sheet properties vary in the machine direction (MD[4]), the cross-machine direction (CD) and the thickness direction (ZD) (see Fig. 2.3).

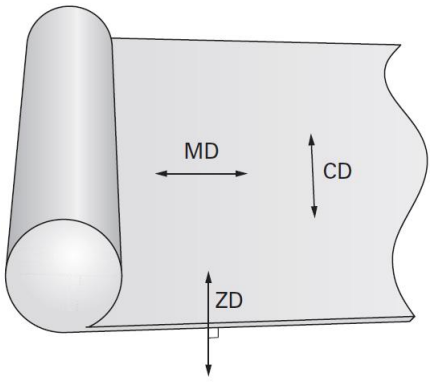

Figure 2.3. Definition of the three directions in paper (Ek et al. 2009).

[4] Machine direction is the direction in which the stock flows onto the paper machine wire.

2.3.1 Pore structure analysis

The structure of the sheet consisting of fibres and pores is determined by the fibre network. The pore size distribution is a key paper property in many processes such as drying, coating and printing.

For paper-like materials, the most important property that the papermaker is usually concerned with is achieving a homogeneous fibre network structure. In the traditional water-forming processing the fibres tend to flocculate. Thus, turbulence in the suspending medium is usually created in order to reduce the flocculation of fibres. Non-uniformity becomes extremely severe for long fibres (the fibre length used for usual paper grades is a couple of millimetres) and/or at high consistency stock. Therefore, studying the role of the suspending medium is extremely important when forming a network structure.

In order to achieve a better understanding between the various processing factors (e.g. fibre consistency, fibre orientation, drainage, wet pressing, drying) and the paper properties, it is highly necessary to obtain knowledge of the pore structure of the paper. There are many techniques to determine the microstructure of porous materials including the 3-d reconstruction approach using X-ray µCT, 2-d imaging techniques such as SEM and light microscopy, or fluid penetration measurement such as mercury intrusion porosimetry, MIP.

A considerable amount of pore structure characterisation in the pulp and paper industry has concerned water-formed samples (Chinga-Carrasco 2009; Goel et al. 2001; Samuelsen et al. 2001; Aaltosalmi et al. 2004; Holmstad 2004), but little research has been done on the structure of foam-formed fibre networks. In conventional water-forming, the pore size distributions obey the log-normal distribution, which means that the amount of large pores is relatively small (Niskanen 2008). On the other hand, a different pore size distribution can be obtained by using foam as the material carrier instead of water (Hjelt et al. 2011; Kinnunen et al. 2013).

Recent studies have shown that a non-invasive technique, X-ray µCT, provides considerable additional information compared to 2-d cross-sectional imaging techniques (Goal et al. 2001; Samuelsen et al. 2001; Holmstad 2004). However, SEM has become more or less the standard tool for researchers in the pulp and paper industry. SEM is available at almost every pulp and paper research institute. Therefore, it is natural to use SEM for studying the paper structure as long as it can provide the structural information of interest. The high resolution achieved by SEM in the low-vacuum mode permits visualisation of pigment particles and interparticle volumes (Chinga-Carrasco 2002). Sample preparation is however time consuming and the structure may distort during the preparation of the cross-sectional samples.

In a recent study by (Hjelt et al. 2011), X-ray µCT was used to evaluate the pore structure of foam-formed and water-formed samples made of chemi-thermomechanical pulp (CTMP). An important conclusion was that the porous structure obtained with foam-forming differs remarkably from that obtained with water-forming.

The capability of mercury intrusion porosimetry (MIP) to evaluate the pore structure in handsheets and commercially available paper made of different kinds of pulp has been demonstrated by (Moura et al. 2005). The main drawback of MIP is that high pressure is needed to force the mercury into the small pores since pressure is inversely proportional to the pore size. This may distort the skeletal porous structure of the sample, in particular when cellulose or latex are present. In addition, large pores may also be shielded by small throats at the surface (Gane et al. 2004).

2.3.2 Porosity

Porosity measures the relative void volume in a material. If a sheet has a ume V, and V_T is the volume occupied by the fibres, then porosity can be expressed in the form

$$\varphi = \frac{V - V_T}{V} = 1 - \frac{\rho}{\rho_f}, \tag{2.13}$$

where ρ is the sheet density and ρ_f is the fibre density.

Porosity of paper can be determined by a variety of techniques. The most commonly used technique is taking cross sections of the sheet and subsequently using image analysis to determine the relative amount of voids in the solid material. Sample preparation may however cause some distortions. The three dimensional (3-d) method of X-ray µCT is now possible for various analyses of the sheet structure.

Vernhes et al. have compared results of X-ray µCT with those of ESEM for paper structure (Vernhes et al. 2008). Lower porosity values were observed with ESEM than with X-ray µCT. They attributed that mainly to sample preparation, where cross-sectional images were distorted. Other researchers (Chinga-Carrasco et al. 2008) have however found that porosity has been lower for the cross-sectional images of X-ray µCT than those of SEM, and for 3-d reconstraction images obtained from water-formed samples of thermo-mechanical pulp. Nevertheless, for small pores the resolution is important, with SEM being capable of much higher resolution than X-ray µCT.

2.4 Mechanical properties

The mechanical properties that are often investigated in paper are the elastic modulus and the tensile index. In the paper industry the term index means that strength is normalised by grammage to get rid of variation in the basis weight of the sample. Figure 2.4 shows a typical stress-strain curve of paper. The concept of stress, *i.e.* force per unit area, is fundamental. In the paper industry, the term tension is usually defined as force divided by width because the thickness is not constant across the paper structure.

Tensile strength is often defined as the maximum force per width of the strip (kN/m). Tensile index is the tensile strength divided by grammage (Nm/kg). Tensile stiffness is the force divided by the elongation and width of the test sample (kN/m). The tensile stiffness is the slope of the linear part of the stress-strain curve. The elastic modulus is the tensile stiffness divided by the thickness of the test sample (MPa).

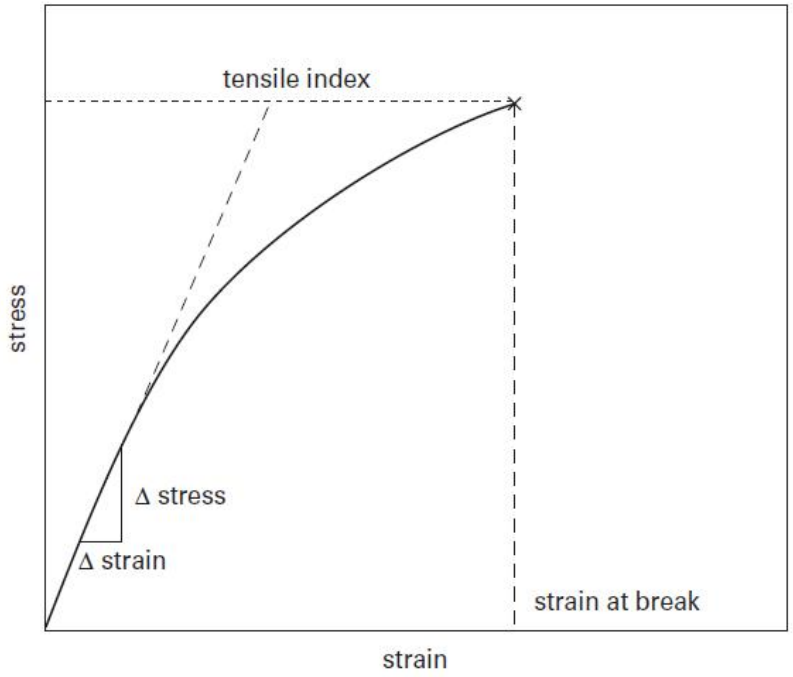

Figure 2.4. A typical stress-strain curve of paper (Ek et al. 2009).

Smith and coworkers (Smith et al.1974) have studied the tensile properties for both water-formed and foam-formed sheets. The densities of the water-formed and foam-formed sheets were respectively 217 kg/m^3 and 185 kg/m^3. The foam-formed sheets had approximately a half of the strength of the water-formed sheets. They attributed loss in the strength to reduction in the consolidating forces during the drying process caused by the presence of surfactant in the foam-formed sheets. They found however that wet pressing and/or beating were very effective ways to regain the strength. The problem with wet pressing and beating is that the obtained bulk is decreased. Kinnunen and coworkers (Kinnunen et al. 2013) addressed the loss in the strength of foam-formed sheets made of kraft and CTMP fibres by adding micro-fibrillated cellulose (MFC) to suspensions, where no

wet pressing was applied to the sheets. Results were astonishing since MFC improved the strength of foam-formed sheets, while still retaining a high bulk structure.

The tensile strength and elastic modulus of water-formed and foam-formed sheets have also been investigated recently by (Lehmonen et al. 2013). Their comparison was carried out at almost equal sheet density. They concluded that the tensile properties of both sheets, made with different forming techniques, were quite similar.

3. Methodology

> You see things; and you say "Why?" But I dream things that never were; and I say "Why not?"
>
> – George Bernard Shaw, Back to Methuselah

In this chapter we describe the experimental and theoretical methods used in this study. The experimental set-up involved foam generation and handsheet preparation. We describe also the surface tension measurements, air content and bubble size measurements and the pore size analysis. Moreover, the physical measurements of the macroscopic sheet properties are also presented. Furthermore, a theoretical derivation of the Sauter mean radius of bubble size is discussed.

3.1 Foam generation

Foam can be made in many different ways (Weaire and Hutzler 1999; Cantat et al. 2013; Exerowa and Kruglyakov 1998). In this Thesis, foam was generated by an axially agitated mixing. Anionic surfactant sodium dodecyl sulphate (SDS) $C_{12}H_{25}SO_4Na$ was added into the liquid before the mixing operation. SDS was obtained from Sigma–Aldrich and had 90% or 99% purity. Most of the mixing experiments were carried out in a transparent cylindrical vessel of a 20 cm diameter (see Fig. 3.1a). Three baffles (cross-section 14 mm × 8 mm) were used to help the foaming process. Another vessel of a 27 cm diameter was used only for studying the impact of shear forces on the bubble size in different parts of the vessel. In this case, shear forces were expected to be smaller due to the larger ratio between the impeller and vessel diameters and the absence of baffles. The rotation speed varied in the range 2000–6900 (RPM). Mixing was carried out long enough (10-30 min) for the air content of the foam to stabilise.

Using one or two impellers in the mixer was not sufficient to draw air into the system, at low rotation speeds in particular. Addition of a third impeller helped to generate the foam. The main benefit of such a set-up was to raise the air content to a high level. Moreover, using this kind of set-up increased the range of different

bubble sizes and extreme rotation speeds that could be used. The lowest impeller was always as close to the vessel bottom as possible, whereas the second impeller was placed always at the initial liquid surface. The third impeller was initially in free air and got involved only after the first two impellers had raised the foam surface high enough so as to reach the third impeller.

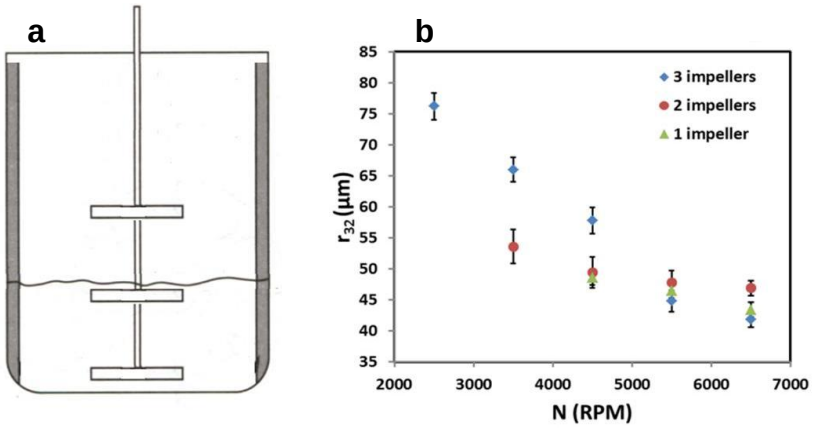

Figure 3.1. a) Side view of the cylindrical vessel that was used in most of the experiments with three impellers. The line shows the initial suspension level when mixing was begun. b) Mean bubble size (Sauter mean radius) as a function of rotation speed N. The air content varied in the interval 66-71%, and the SDS concentration was 0.2 g/l at 90% purity. (Paper I)

The Sauter mean bubble radius obtained for one, two and three impellers is shown in Fig. 3.1b. The distance between the impellers was 4 cm. The SDS concentration was 0.2 g/l. In spite of quite similar air contents (between 66% and 71%), bubble sizes were strongly influenced by the number of impellers. This indicates that the average shear rate in the foam is not only controlled by the rotation speed, but also by the geometrical arrangement of the experiment.

It is worth mentioning here that whenever the SDS concentration is mentioned in this Thesis without mentioning its purity, it refers to 90% purity. Otherwise, the purity of SDS will be mentioned explicitly in the text.

3.2 Surface tension measurements

The static surface tension at the air-water interface was measured of the suspension using a narrow capillary tube of 0.7 mm radius. The SDS concentration was between 0.005 and 10 g/l. The surface tension was measured several times for each concentration and results were fitted by the Szyszkowski equation (Rosen 2004),

$$\sigma = \sigma_w - \Gamma_{\mathrm{m}} RT \ln(1 + K_L c_s), \tag{3.1}$$

where σ is the surface tension of the suspension, σ_w is the surface tension of pure water, c_s is the bulk surfactant concentration, Γ_m is the maximum amount that can be adsorbed at the interface, K_L is the Langmuir equilibrium adsorption coefficient, T is the absolute temperature and R is the gas constant.

In addition to the static surface tension measurments, the dynamic surface tension for a varying bubble life time was also measured using a BPA-800P bubble pressure tensiometer (KSV Instruments Ltd., Helsinki, Finland) for the 99% and 90% SDS purities at a concentration of 0.3 g/l. Furthermore, the dynamic surface tension for a varying bubble life time was measured at 0.2 g/l SDS concentration and at 99% purity. The dynamic surface tensions were also obtained by adding 0.33% refined kraft fibres and 0.33% rayon fibres to suspensions which contained 0.2 g/l SDS at 99% purity.

3.3 Fibre materials

The fibres used in this study were natural or regenerated fibres, see Fig. 3.2. The natural fibres were unrefined bleached kraft[5] (denoted below as kraft U, SR 18[6]), (pre-)refined bleached kraft (kraft R, freeness 607 ml) or chemi-thermo-mechanical (CTMP, freeness 570 ml) fibres, whereas the regenerated fibres were Lenzing viscose staple (viscose L), Kelheim viscose staple (viscose K) or rayon fibres. The basic properties of the fibres studied are provided in Table 3.1.

Viscose and rayon fibres had a density of approximately 1500 kg/m^3, which is close to that of pure cellulose. The natural fibres had however a lower density, approximately 1000 kg/m^3, because natural fibres include a lumen which is an open core of the fibre.

The reason for using regenerated fibres is that the fibre length can then be controlled. This is impossible to achieve with natural fibres for which a distribution of fibre lengths is always present. The regenerated fibres have smooth surfaces, whereas the natural fibres have rough surfaces and they are associated with fine particles.

[5] Kraft is German word for ''strength''. The German developer Carl Dahl called his invention the kraft process because of the superior strength of the resulting paper.

[6] SR (Schopper-Riegler) number and freeness both indicate the dewaterability of pulp suspension.

Table 3.1. The basic properties of the fibres used in this study.

Fibre type	rayon	viscose L	viscose K	kraft U/R	CTMP
Length (mm)	0.35	10	6.0/3.0	2.3	1.6
Width (µm)	13	18	20	35	26
Coarseness (mg/m)	0.19	0.17	0.17	0.14	0.22

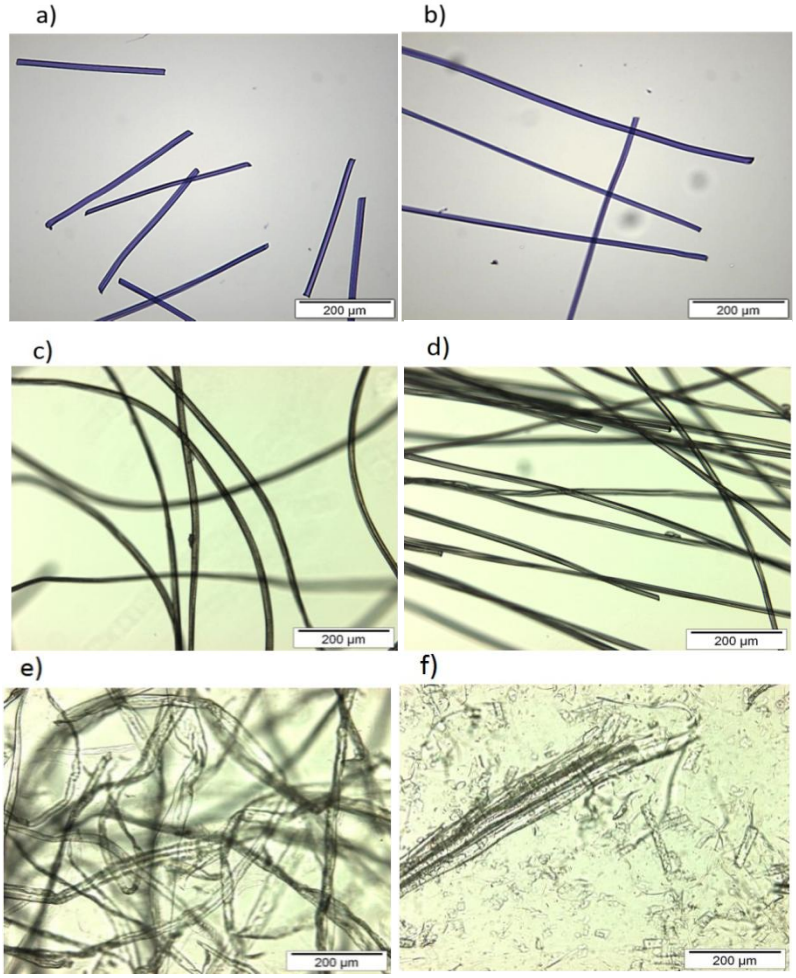

Figure 3.2. Light microscope images of different types of fibre used in the study: (a) rayon (0.35 mm), (b) rayon (1.0 mm), (c) viscose L, (d) viscose K, (e) kraft R, (f) CTMP.

3.4 Air content and bubble size measurements

Air content was obtained by determining the total foam volume and the initial amount of water used to generate the foam. The volume could be read out from the vessel scale immediately after mixing was stopped.

A narrow gap between two glass plates was used to collect the foam samples (see Fig. 3.3). The distance between the two glass plates was 1.6 mm. Foam samples were collected by dipping the cuvette into the foam. Then images of the foam were taken with a CCD camera within 10-20 seconds after taking the sample. Resolution of the images was 2448 x 2048 pixels and its typical absolute size was 1.8 x 1.5 mm. For wet foam the bubbles usually were of a spherical shape and determining their radius was an easy task. The number of measured bubbles varied between 250 and 2000. The Sauter mean radius was usually used to describe the foam properties rather than the arithmetic average. The Sauter mean radius can be defined such that

$$r_{32} = \frac{\sum r^3}{\sum r^2}, \tag{3.2}$$

where r is the bubble radius.

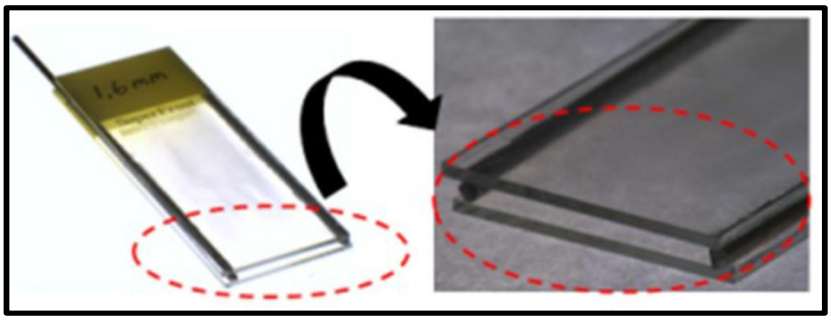

Figure 3.3. Cuvette used for collecting the foam samples with a 1.6 mm spacing between the two glass plates (Lappalainen and Lehmonen 2012).

3.5 Hand sheet preparation

The procedure of making a foam-formed handsheet is shown in Fig. 3.4. The area of the related handsheet mould was 0.1 m^2, and the target grammage of the handsheets was 100 g/m^2. The forming fabric was set onto a fixed position with the help of some water and it was fitted tightly to the edge of the mould (Fig. 3.4a). The lid was closed and locked tightly, the metal plate set in a position, where the 5 mm gap between the plate and the wall stayed constant throughout the whole series (Fig. 3.4b). When a steady state of the foam-fibre mixture was achieved, the mixture was quickly decanted into the handsheet mould (Fig. 3.4c). Then the metal plate was removed by sliding it rightwards and slightly pushing against the foam to even out its surface level. The mixture surface was covered with a vinyl sheet. After the foam was settled, it was filtered through the forming fabric using a vacuum chamber (0.5 bar vacuum initial dewatering) (Fig. 3.4d). The vinyl sheet was removed from top of the surface (Fig. 3.4e), and a supported fabric was put onto the wet sheet (Fig. 3.4f), the smoother side against the sheet. Then the wet sheet with the two fabrics was transferred from the mould to a special suction table for pre-drying (Fig. 3.4g). Suction table had a slit 5 mm wide, and air was sucked through the sheets through this slit with 0.2 bar vacuum. The wet sheet was slid over the suction slit for 5 times. Then, the upper fabric was removed carefully (Fig. 3.4h). The wet sheet was kept temporarily between aluminium foils. Wet sheets were finally transferred to plates covered with another fabric to be dried in an air tunnel for one night at 23°C, 50% relative humidity (Fig. 3.5).

The water-formed handsheets were made of the same fibre materials as the foam-formed handsheets. The target grammage was 100 g/m^2. The sheets were made with a standard handsheet mould. The process was exactly the same except that there was no vacuum during the filtration process. The same forming fabric was used during the filtration process as for the foam-formed sheets. The size of the sheets was 16.5 cm x 16.5 cm. The initial consistency was 0.045%.The pre-drying on the suction table and final drying in the air tunnel were carried out in the same way as for foam-formed handsheets.

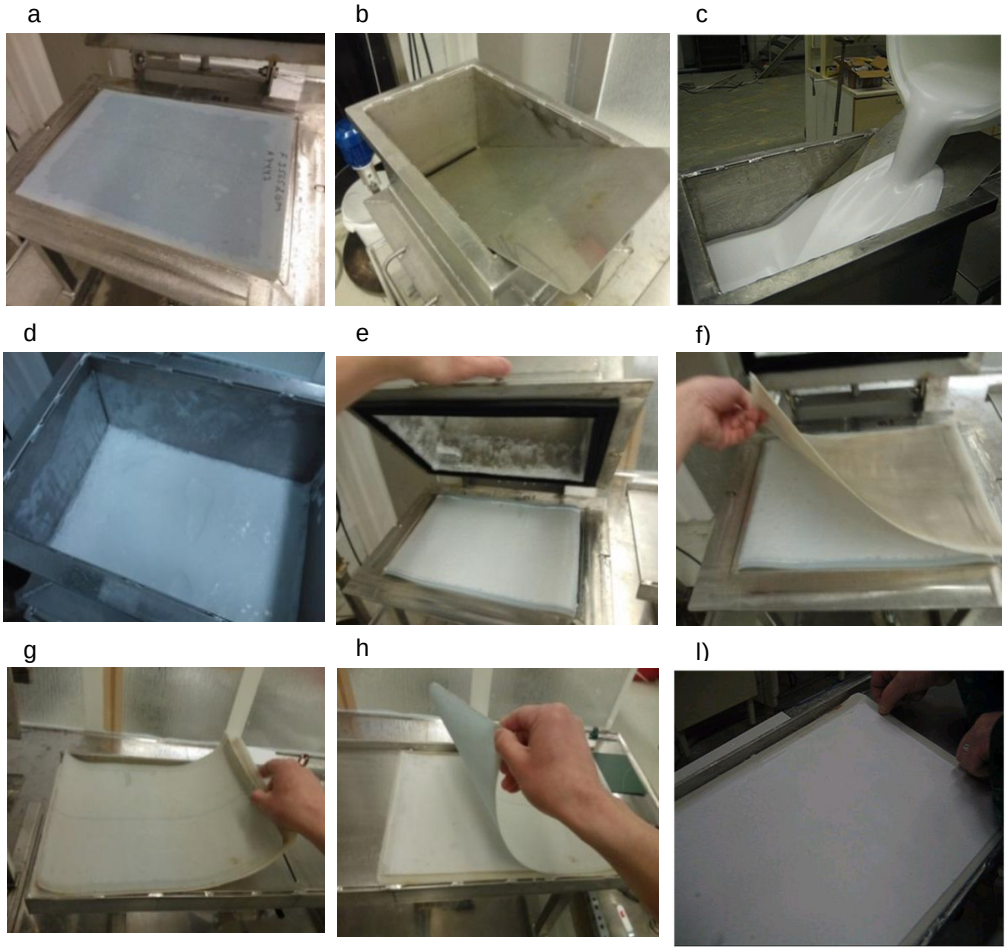

Figure 3.4. A schematic diagram of the foam-formed handsheet making process.

Figure 3.5. The drying process of a foam-formed handsheet.

3.6 Sheet properties

3.6.1 Basic sheet properties

The grammage (basis-weight), thickness and density of both water-formed and foam-formed handsheets were measured. The grammage of the sheets was determined according to the standard method ISO 536. The thickness measurements were carried out with a Lorentzen & Wettre device. This device avoids pressing of the sheet during the measurement. Thickness was obtained as the average of 10 measurements for each sheet. These measurements were done at an equal spacing between the measurement points in order to represent the whole area of the sheet. In order to determine the density of each sheet, their grammages were divided by thicknesses. In the paper industry, the inverted density is often used, which is called the bulk, usually given in cm^3/g.

3.6.2 Macroscopic sheet properties

Tensile strength: The tensile strength measurements of the handsheets were performed with an Alwetron TH1 horizontal tensile tester in accordance with ISO 1924-2. 12 strips of 15 mm width were tested from each handsheet. Six strips were cut in the machine direction (MD) and six in the cross-machine direction (CD).

Air permeability: The air permeability measurements of the handsheets were performed with a Lorentzen & Wettre SE114 device in accordance with ISO 8791-2. These measurements were based on the amount of air flow in the surface structure of the sheet. Sample was placed on a glass plate under a weight with a hole in the circular measurement area. Ten parallel measurements for each side of the sample were done separately. The measurement range of this Bendtsen tester was 0 to 3500 ml/min.

Opacity: The opacity measurements were performed with a Lorentzen & Wettre SE070R Elrepho spectrophotometer in accordance with ISO 2471.

3.7 Pore structure analysis

3.7.1 X-ray micro-computed tomography

The non-invasive X-ray µCT technique was employed for assessing and characterising the structure of the foam-formed and water-formed sheets. The first commercial X-ray tomography device was developed by Hounsfield in 1971 (Bock and Jacobi 2013) for medical imaging. After this tomography became a very popular method in medical science. Now this technique has been reported to successfully depict paper samples in 3-d with a relatively high resolution (Holmstad 2004).

In this study we used the data obtained by X-ray µCT as a benchmark for other characterisation techniques. µCT used for the measurements was an Xradia Micro-XCT-400. The device used a standard X-ray tube.

Imaging was performed for 2 mm x 3 mm sample regions. The imaged area was chosen in a region located a bit away from the edge of the sample to minimise the effect of the inhomogeneity near the border. Image was taken with a 1.1 µm resolution in all directions.

3.7.2 Sample preparation for cross-sectional imaging

There are several techniques for obtaining the cross-sectional images such as those of a scanning electron microscope SEM, transmission electron microscope TEM and light microscope LM. In this study SEM and LM were used for assessing the pore structure of the sheets.

Sample preparation was extremely important for cross-sectional image analysis. It was highly important that sample preparation was performed carefully in order to access the detailed sheet structure. The sample preparation involved embedding the paper sample in epoxy resin under vacuum. The idea behind this method was to give a rigid support to the paper structure.

In this study samples 25 mm long were embedded in epoxy resin. After hardening of the resin, cross-sectional surfaces were made by grinding and polishing. Then, these cross-sections were examined under SEM. The resolution used was 0.56 µm per pixel, and 4 images were taken from each sample.

For LM, the samples were embedded in epoxy and then cross-sections were cut by microtome to produce thin slices. The resolution was 1.37 µm per pixel, and 4 images were taken from each sample.

3.7.3 Direct surface imaging

Direct images of the sheet surfaces were taken with a CCD camera. The number of pixels in the CCD elements was 2448 x 2048 and the typical absolute size of the image was 1.8 x 1.5 mm. Figure 3.6 shows examples of surface images taken with the CCD camera for foam-formed sheets made of kraft and CTMP fibres at 2000 RPM. The number of parallel images was 8.

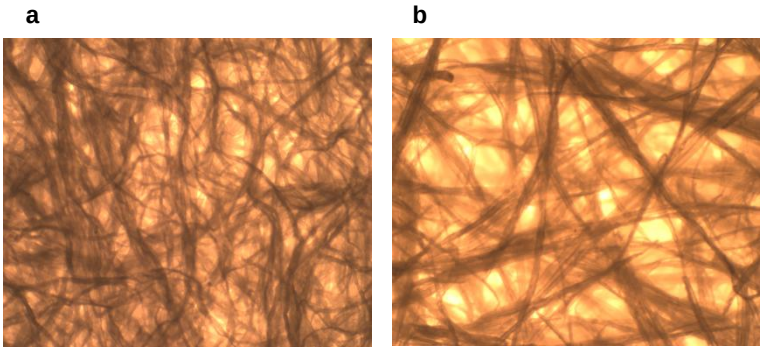

Figure 3.6. Images of foam-formed sheet surface made at 2000 RPM of (a) kraft and (b) CTMP fibres. The size of the images is 1.8 mm x 1.5 mm.

3.7.4 Mercury intrusion porosimetry

Mercury is a non-wetting liquid, thus an external pressure is needed to force mercury into porous samples. A high pressure is required to intrude mercury into small pores, whereas a low pressure is required for mercury to intrude a large pore, since pressure is inversely proportional to the pore size. In this study the applied pressures varied between 0.014 and 400 MPa so as to force mercury into the sample. The contact angle and the surface tension used for all tests were respectively 140^{o} and 0.48 N/m.

3.8 Determination of the pore size distribution

A MATLAB routine developed at VTT was used for characterisation of the void structure. First, the interested area was cropped (Fig. 3.7a). Then, the grey-scale image was converted to a binary image by interactive thresholding. After that, a distance transform (Rosenfeld and Pfaltz 1966) was done of the image. For each pixel, the distance transform assigns a number that is the distance between that pixel and the nearest black pixel corresponding to the material. Finally, the void space was filled by circles of maximal radius using results of the distance transform (Fig. 3.7b).

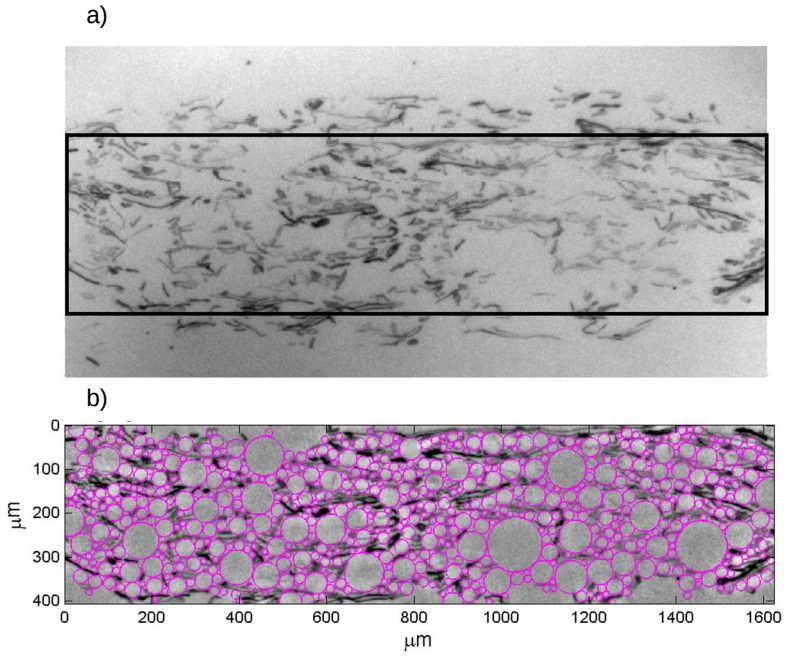

Figure 3.7. a) A light microscope image of a kraft sheet at 2000 RPM. b) Filling the void space of the cropped area by circles of maximally large radii using the results of the distance transform. (Paper IV)

For X-ray µCT, the volume-weighted pore size distribution was derived from determination of the local thickness, see Fig. 3.8. The local thickness at each point represents the diameter of the largest sphere that fits inside the void space and contains the point. More complete descriptions of this method are given in (Hildebrand and Rüesgsegger 1996; Saito and Toriwaki 1994).

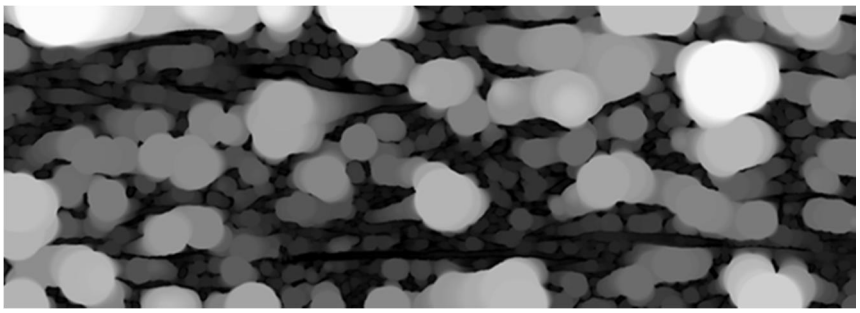

Figure 3.8. Local thicknesses in a 3-d rendered image (xz cross-section) for a CTMP sheet made with foam-forming, foam made at a rotation speed of 2000 RPM. Some fibres are visible as long horizontal objects. (Paper IV)

3.9 Theoretical model for the mean bubble size

The aim of this section is to derive a single formula that can explain the average behaviour of the mean bubble size in mixing flows. Before using Eq. (2.9) as a starting point to our derivation, its modification is needed in order to replace the shear rate with the rotation speed. According to (Metzner and Otto 1957) the characteristic shear rate can be related to the rotation speed such that

$$\dot{\gamma} = kN, \tag{3.4}$$

where k is a constant which depends on the mixing geometry and the fluid rheology. Metzner and Otto (Metzner and Otto 1957) suggested that k was approximately 13. Moreover, we assume that flow index *n* is unity in Eqs. (2.11) and (2.12), which means that dependence of the viscosity of foam on its shear rate can be neglected. Thus Eq. (2.9) becomes

$$r_{32} \sim \frac{\sigma}{\mu N}. \tag{3.5}$$

This equation tells us that the average bubble size depends on surface tension and the inverse of rotation speed of the mixer. Figure 3.9a displays the average bubble radius plotted against the inverse of rotation speed for different SDS concentrations. It is evident that the linear trend between the average bubble size and the inverse of rotation speed does not work for high rotation speeds. Thus, Eq. (3.5) does not describe the bubble size at a high rotation speed. Figure 3.9b displays the average bubble radius plotted against the surface tension. It is evident that for a high rotation speed such as e.g. 6400 RPM, the mean bubble size is decreased when the surface tension is increased. Therefore Eq. (3.5) obviously needs (an) additional refinement(s).

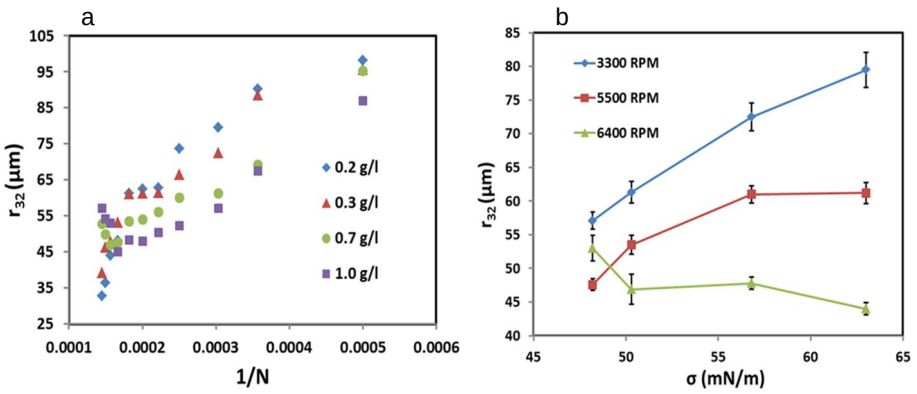

Figure 3.9. The mean bubble size for several SDS concentrations plotted against a) the inverse of rotation speed and b) surface tension. (Paper I)

The effect of air content on bubble size is missing in Eq. (3.5), although it plays an important role in determining the average bubble size. In order to understand the effect of air content, the mechanisms of surfactant in stabilizing the bubbles should be understood. When a bubble is deformed, surfactant molecules start to stabilise the underlying deformation (Rosen 2004). As the bulk surfactant concentration is increased, the amount of active surfactant molecules becomes larger. This means that bubbles sustain higher deformations (Rosen 2004). However, the amount of active surfactant molecules is affected by the total interfacial area, which is obviously affected by the air content.

In the following we determine the effect of air content on the interface surfactant concentration and relate that to bubble size.

First notice that the Sauter mean radius can be expressed in the form

$$r_{32} = \frac{\sum r^3}{\sum r^2} = \frac{3\phi V_T}{A_I}, \tag{3.6}$$

where ϕ is the air content, V_T is the total volume of the system and A_I is the total interface area of bubbles. The amount of surfactants is divided between the bulk liquid and the interfaces. For the initial suspension before mixing, the total surfactant mass is $c_s(1-\phi)V_T$, where c_s is the initial bulk surfactant concentration. Now, the mass balance equation for the surfactants is given by

$$c_s(1-\phi)V_T = \Gamma A_I + c_f(1-\phi)V_T, \tag{3.7}$$

where Γ is the average concentration of excess surface surfactants and c_f is the surfactant concentration in the liquid phase. The initial bulk surfactant concentration is assumed to be below the critical micelle concentration. From Eqs. (3.6) and (3.7) we can now conclude that

$$(c_s - c_f)(1-\phi) = \frac{3\Gamma\phi}{r_{32}}. \tag{3.8}$$

The Langmuir isotherm can be expressed by (Rosen 2004)

$$\frac{\Gamma}{\Gamma_m} = \frac{K_L c_f}{(1+K_L c_f)}, \tag{3.9}$$

where K_L and Γ_m are constants. For small c_f, the surface concentration is approximately given by $\Gamma \approx K_L \Gamma_m c_f$. Thus, Eq. (3.8) can be expressed in the form

$$(c_s - c_f)(1-\phi) = \frac{3\Gamma\phi}{r_{32}} \approx \frac{3K_L\Gamma_m c_f \phi}{r_{32}}. \tag{3.10}$$

Rewriting Eq. (3.10) such that

$$r_{32} \approx \frac{3c_f K_L \Gamma_m \phi}{(c_s - c_f)(1-\phi)}. \tag{3.11}$$

In this equation c_f follows $c_s - c_f$ for the steady state because the steady state is always associated with finite values of the air content and bubble size. The leading effect of air content on bubble size is thus given by

$$r_{32} \sim \frac{1}{\frac{1}{\phi} - 1}. \tag{3.12}$$

Combining Eqs. (3.5) and (3.12) and assuming that viscosity varies only little in the range of rotation speed used in this study, we find that

$$r_{32} \sim \frac{\sigma}{N(\frac{1}{\phi} - 1)}. \tag{3.13}$$

4. Results and discussion

“Knowledge is the only instrument of production that is not subject to diminishing returns.”

— J. M. Clark, Journal of Political Economy, Oct. 1927

The main results obtained in this work were organised into four parts. The first two parts present the properties of pure foams and fibre laden foams. In the last two parts, comparison of the structure of sheets made with foam-forming and water-forming is presented.

4.1 Foam properties without fibres

4.1.1 Bubble size in different parts of the vessel

In order to study the effect of shear on the bubble size, we took foam samples from different parts of the vessel during mixing. A vessel of 27 cm diameter was used as it allowed the easiest control of the place, where the sample was taken. Figure 4.1 shows the different locations around the second impeller:

1. near the impeller
2. between the impeller and the wall
3. at the wall
4. above the impeller
5. near the stirrer shaft.

The mean bubble size seemed to be affected by shear forces that varied at different locations, as shown by Figs. 4.2 and 4.3. The bubble size was quite similar near the impeller (location 1) and further towards the wall, (2). At the wall however (3), the bubble size looked more even with slightly smaller mean size than at the locations 1 or 2. On the other hand, above the impeller (4), both small and large bubbles appeared perhaps due to break up of large bubbles due to shear forces

caused by the flow passing the impeller. The mean bubble size was also smallest at the location 4.

It can be concluded that foam properties are not homogeneous in a mixer, especially near impellers, even after the air content has been stabilised. In all further analyses, we always tried to take the samples at roughly the same location (essentially above locations 4 and 5), well away from the topmost impeller.

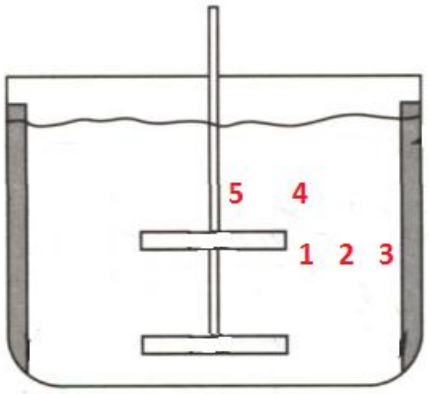

Figure 4.1. Different locations of the vessel, at which foam samples were taken.

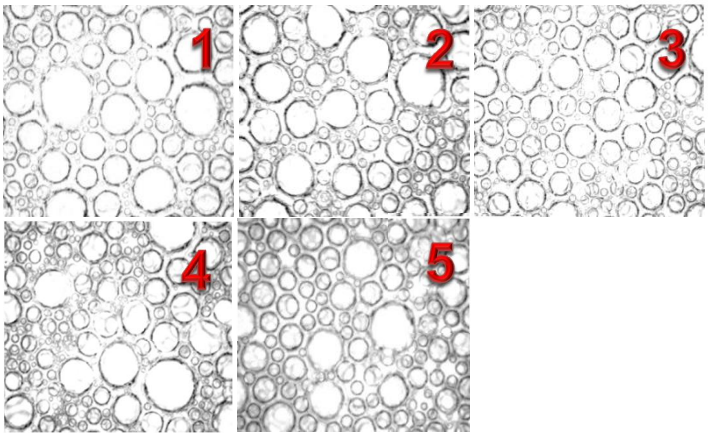

Figure 4.2. Images of foam at different locations for 2800 RPM.

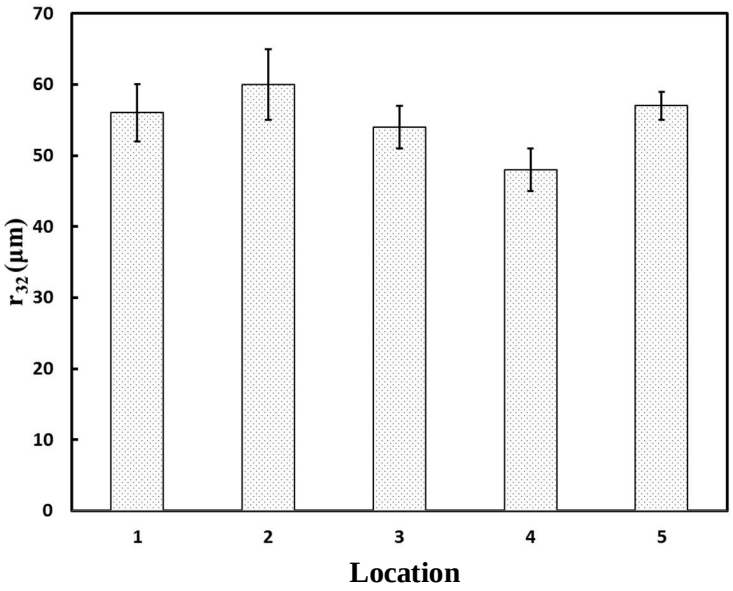

Figure 4.3. The mean bubble size at different locations for 2800 RPM. The SDS concentration was 0.2 g/l.

4.1.2 Variations in the air content and mean bubble size at different flow regimes

In the following, we study how the air content and mean bubble size are affected by the type of flow, rotation speed and the surfactant concentration.

Figure 4.4a displays the air content of the foam plotted against the rotation speed for different SDS concentrations. The SDS concentrations were well below CMC. It is evident that air content is insensitive to the SDS concentrations as long as the rotation speed in mixing is below 5500 RPM. Above 5500 RPM, a dramatic change happened in the air content: it became strongly sensitive to the SDS concentration. Above 5500 RPM, the air content increased with increasing rotation speed. The air content can also drop at a low SDS concentration however.

Below 5500 RPM, the macroscopic flow of the foam was quite stable and there were no small vertices on the surface of the foam. Situation was totally different above 5500 RPM however, where flow patterns were chaotic with vertices on its surface (see Fig. 4.5). The characteristic shear rate for the onset of macro-instabilities, given by Eq. (3.4), is $\dot{\gamma}$~1000 1/s. The corresponding characteristic shear viscosity of the foam can be estimated to be around 50 mPa s (Gardiner et al. 1999). The critical Reynold number therefore for the onset of macro-instabilities

is Re~3500. Despite the differences with the previous studies (Nouri and Whitelaw 1990; Hasal et al. 2008) in terms of the mixing geometry and fluid rheology, the critical Reynold number for the onset of macro-instabilities is close to the values given in these studies.

Figure 4.4b displays the average bubble size of the foam plotted against the rotation speed for different SDS concentrations. Below 5500 RPM the average bubble size decreases with increasing rotation speed and with decreasing surface tension. Above 5500 RPM the average bubble size increases with increasing SDS concentration and with increasing rotational speed for a few highest SDS concentrations.

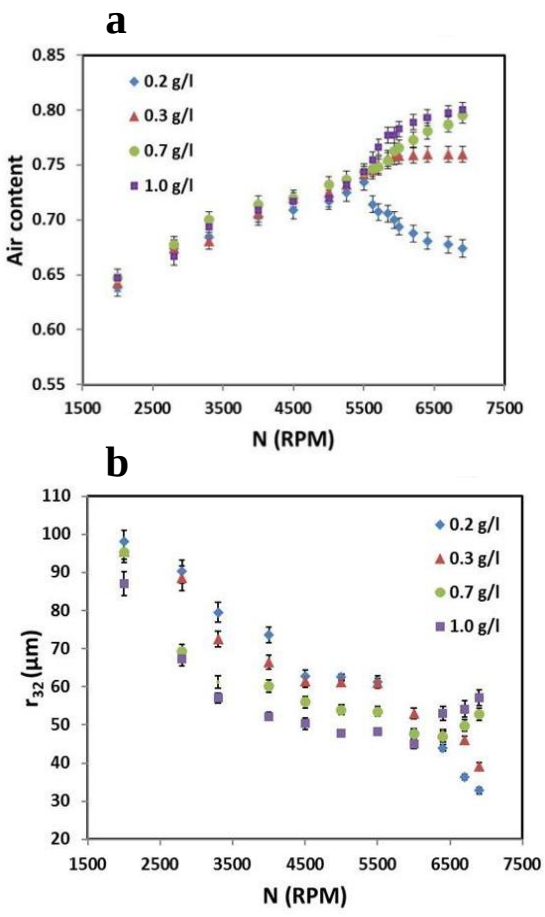

Figure 4.4. Air content (a) and average bubble radius (b) as the function of rotation speed (N). In the stable flow regime (below 5500 RPM), the air content was quite insensitive to the surfactant concentration, whereas in the unstable region

(above 5500 RPM) the air content depended strongly on the surfactant concentration. (Paper I)

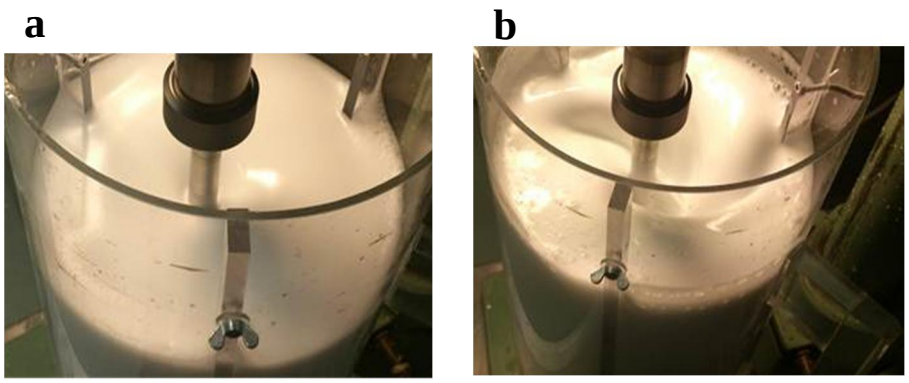

Figure 4.5: The macroscopic flow of the foam during mixing, a) below and b) above 5500 RPM. Below 5500 RPM the macroscopic flow of the foam was quite stable and no vertices appeared on the surface, whereas above 5500 RPM its surface flow became unstable.

Figure 4.6 shows images of bubbles at rotation speed 6700 RPM for 0.7 g/l and 0.2 g/l SDS concentrations. The air contents were 0.79 and 0.68 respectively for the 0.7 g/l and 0.2 g/l SDS concentrations. Bigger bubbles were obtained for higher SDS concentrations with a non-spherical shape. For lower SDS concentrations the bubbles were smaller and quite spherical.

The surface tension can be lowered by addition of surfactant, thus bubble size should be smaller. This is not the case here however. SDS molecules moved along the bubble interfaces in such a way that their concentration gradients balanced possible bubble deformations. For high SDS concentrations above 5500 RPM bubbles were easier to deform because of a smaller surface tension. For SDS, bubbles could withstand higher deformations before they broke, and hence the shape of these bubbles became closer to hexagonal.

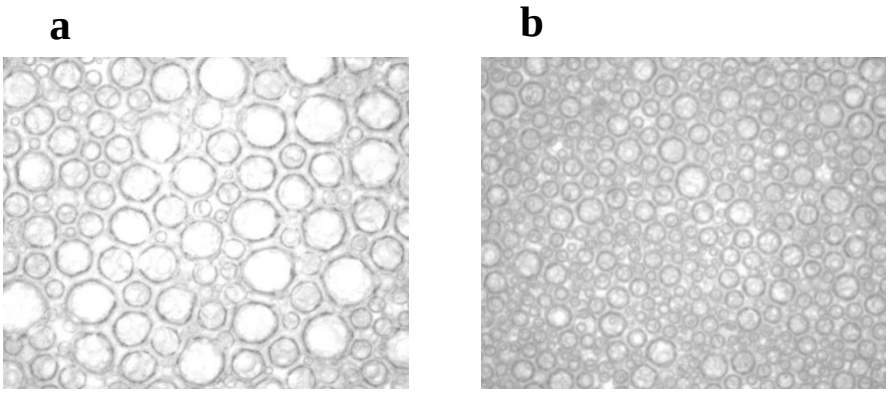

Figure 4.6: Images of bubbles at rotation speed 6700 RPM for SDS concentrations of a) 0.7 g/l and b) 0.2 g/l. The respective air contents were 0.79 (a) and 0.68 (b). The size of the images is 1.8 mm x 1.5 mm. (Paper I)

4.1.3 The behaviour of air content and mean bubble size at different SDS purities

Figure 4.7 shows the effect of SDS purity on the air content and mean bubble size. SDS concentrations were 0.2 g/l and 0.3 g/l. The air content at both SDS purity levels increased with increasing rotation speed until the onset of macro-instabilities occurred. The locations of these onsets of macro-instabilities were different for different SDS purities. For the higher (99%) SDS purity the onset occurred for 0.2 g/l and 0.3 g/l SDS concentrations respectively at 6000 RPM and 6700 RPM. The drop in the air content was sharp for 0.2 g/l. This decay was associated with the reduction of the mean bubble size. A similar decrease in the air content and mean bubble size happened for 0.3 g/l.

This behaviour of air content and average bubble size was probably caused by adsorption kinetics at the air-water interfaces. The lower surface active impurity reduced the free energy of the system and hence increased the bubble stability (Gonzenbach et al. 2006). A lower SDS purity resulted in a higher amount of surface active impurities absorbed at the air-water interfaces. Surface tension was decreased by absorption of impurities.

It seems that the dynamic surface tension (Fig. 4.8) is probably more important at high rotation speeds than the static surface tension. The processes of bubble formation and break-up are fastest near the impellers. A high rotation speed not only increased the shear rate, but also caused bubbles to enter the impeller region more frequently. For a short bubble life time below 0.5 s, the measured surface tensions were almost equal for both purities. For longer bubble life times, diffusion of impurities to bubble interfaces reduced however the interfacial energy. The resulting drop in the surface tension was stronger for the lower SDS purity. More-

over, the complex coupling of the macroscopic flows in the vessel with foam viscosity, and thus with the air content, gave additional complication in understanding the behaviour of such systems. The Reynold number was decreased with increasing viscosity because of increase in the air content. This on the other hand could reduce the shear rate and stabilize the flow.

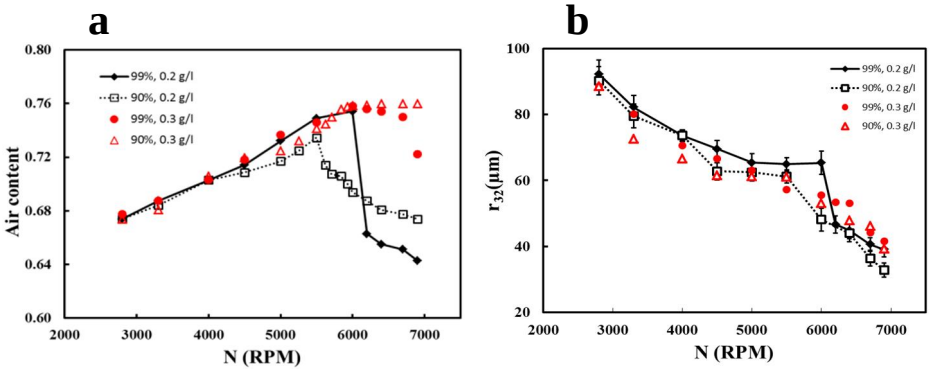

Figure 4.7: Air content (a) and mean bubble size (b) of the pure foam for a varying rotation speed (N). SDS purities and concentrations were 99% and 0.2 g/l, 90 % and 0.2 g/l, 99% and 0.3 g/l, and 90% and 0.3 g/l. The estimated absolute error in the air content measurement was ±0.01. For the mean bubble size, the standard error of the mean is indicated. (Paper II)

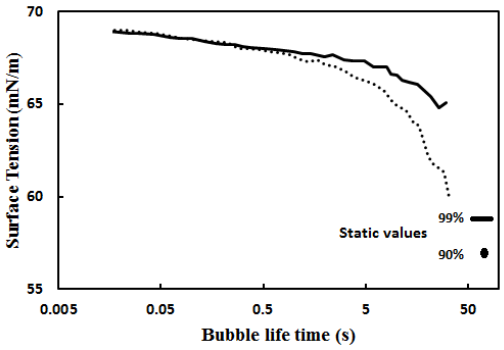

Figure 4.8: Dynamic surface tension for a varying bubble life time as measured with a BPA-800P bubble pressure tensiometer (KSV Instruments Ltd., Helsinki, Finland) for 99% (solid curve) and 90% (dotted curve) SDS purities at a concentration of 0.3 g/l. We also indicate the static surface tensions for both purities. For the 99% purity, the static value was measured using a Sigma 701 force tensiometer (Attension, Espoo, Finland). For the 90% purity, the capillary method was used. (Paper II)

Figure 4.9 shows the measured bubble size in comparison with Eq. (3.13) for both purities. The bubble size was well predicted with Eq. (3.13). The pre-factor was slightly higher for the higher purity.

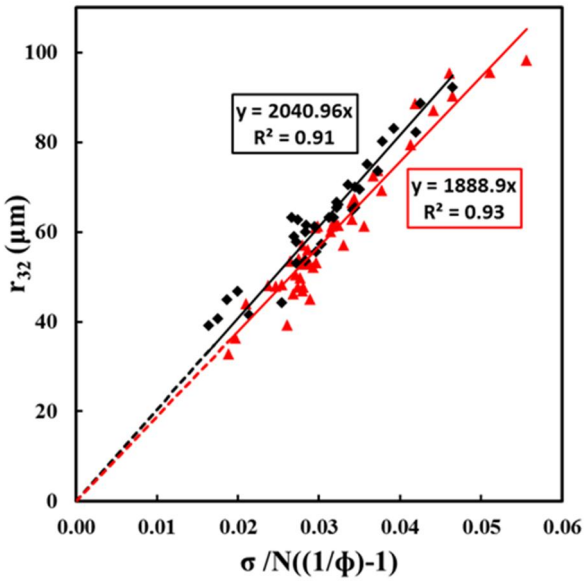

Figure 4.9: The bubble size versus Eq. (3.13) for both SDS purities, 99% (diamonds) and 90% (triangles). (Paper II)

4.2 Properties of foams laden with fibres

In the following, we study the effect of addition of cellulose-based fibres on the foam properties. We start with a general picture with a large set of data. These data have been obtained for varying fibre type, fibre length, consistency and SDS purity. Later the effects of certain fibre properties are studied more closely.

Figure 4.10a shows the air content plotted against the rotation speed for different fibre laden foams. The behaviour of air content in the stable region, *i.e.* below 5500 RPM, was quite similar to that without fibres. This behaviour was rather similar for almost all types and consistencies of the fibre, and for SDS concentrations and purities. The macro-instability behaviour began a bit earlier than for the pure foam, roughly between 5000-5500 RPM. The location of the onset depended

on the fibre type and consistency. Above this speed range, the air content behaviour for most regenerated fibres was similar to that of the pure foam at 90% SDS purity.

Figure 4.10b shows the corresponding bubble size as a function of rotation speed. Variation in the bubble size was much wider than in the air content, below the onset of macro-instabilities in particular. When natural fibres were included in the foam, the mean bubble size in the stable region was below that for the pure foam. When the foam was laden with regenerated fibres, its mean bubble size was sometimes larger than for the pure foam, but there were some cases, where regenerated fibres reduced the mean bubble size in the same way as the natural fibres. We did not try to analyse this behaviour any further.

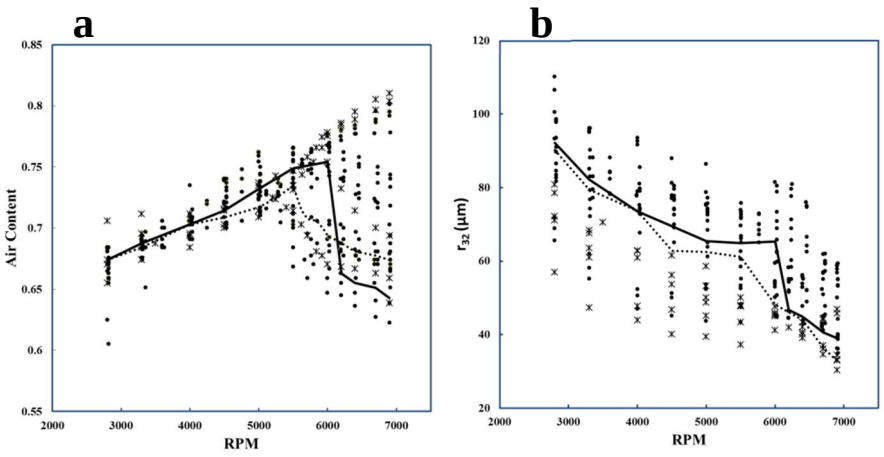

Figure 4.10: Air content (a) and mean bubble size (b) as functions of the rotation speed for all fibres, consistencies, surfactant concentrations and SDS purities studied. The solid circles show data for regenerated fibres (viscose, rayon), and similar data for natural wood fibres (kraft, CTMP) are shown by the crosses. The data for the pure foam at 0.2 g/l SDS concentration are shown with solid (99% purity) and dotted (90% purity) lines. (Paper II)

In the following, the behaviour of wet foams in response to adding natural or regenerated fibres is discussed in more detail.

Figure 4.11 shows the effect of surface properties of the fibres on the air content and mean bubble size of the foam. Comparison is made of refined kraft fibres with viscose fibres at 0.66% fibre consistency and 0.3 g/l SDS concentration. The average fibre lengths were respectively 2.3 and 3.0 mm of the kraft and viscose fibres. The kraft fibres have rough surfaces, whereas the viscose fibres have smooth surfaces. An additional feature of the kraft fibres was that they were associated with approximately 10% of fibrillar fines in the suspension.

In Fig. 4.11a, the air content was quite similar for the two types of fibre in the stable region. For both types of fibre it was slightly below the one for pure foam. At 6000 RPM, where the macro-instability occurs, a big difference was observed in the air contents of these fibres: The difference was around 0.08 per cent units. The mean bubble size was however more or less equal at this speed. In general, the mean bubble size in the stable region was smaller for the kraft than viscose fibres (Fig. 4.11b). Nevertheless, the difference was reduced at higher rotation speeds in both the air content and mean bubble size.

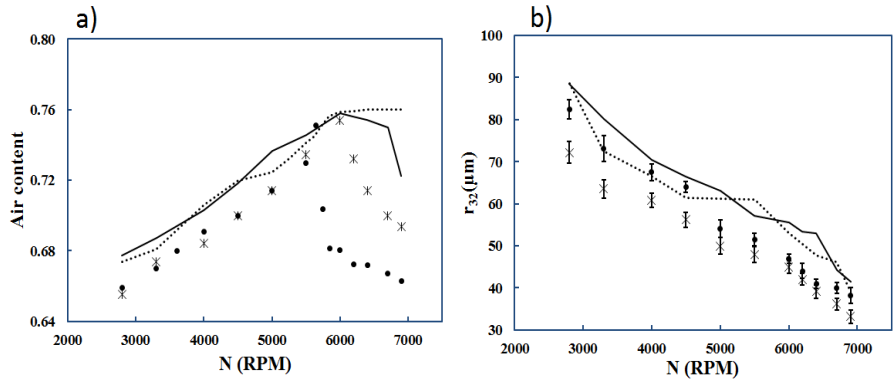

Figure 4.11. Air content (a) and mean bubble size (b) for viscose K (circles) and Kraft R (crosses) fibres at 0.66% consistency and 0.3 g/l SDS concentration. Fibre properties are given in Table 3.1. The data for the pure foams are shown by the solid (99% SDS purity) and dotted (90% purity) lines. (Paper II)

Figure 4.12 shows images of foam with viscose and kraft fibres at 4000 RPM. The SDS concentration was 0.3 g/l. Polydispersity in bubble size was observed in the foam laden with viscose fibres, whereas almost no big bubbles were observed in the foam laden with kraft fibres. The area-weighted bubble size distributions for the pure foam, the foam laden with viscose fibres and the foam laden with kraft fibres are shown in Fig. 4.13. The bubble size distributions of the pure foam and the foam laden with viscose fibres were quite broad with almost no effect of addition of viscose fibres to the distribution. On the other hand, addition of kraft fibres made this distribution narrow. This result is important since it has an impact on the industrial foam processes.

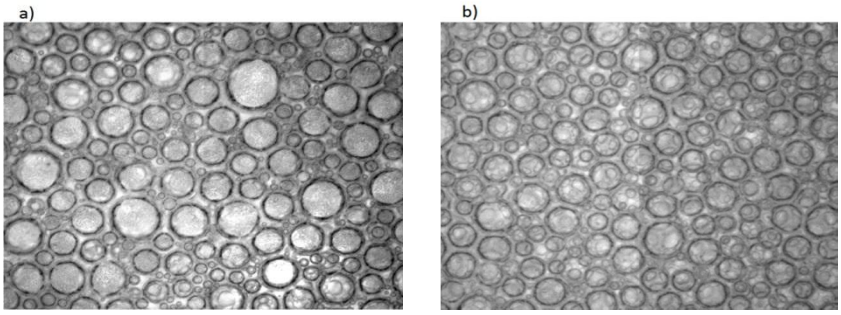

Figure 4.12. Examples of bubble images for foams laden with a) viscose K and b) Kraft R fibres at the rotation speed 4000 RPM and SDS concentration 0.3 g/l. (Paper II)

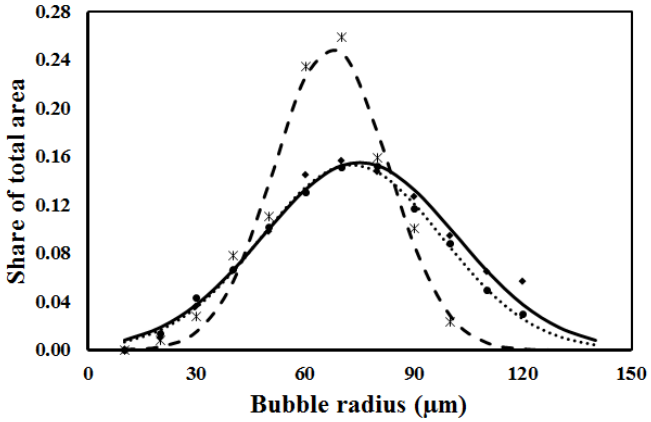

Figure 4.13: Area-weighted bubble size distribution for the pure foam (diamonds, solid curve), the foam laden with Kelheim viscose fibres (circles, dotted curve) and the foam laden with refined kraft fibres (crosses, dashed curve). The rotation speed was 4000 RPM and SDS concentration 0.3 g/l. The curves are Gaussian distributions resulting from fits of the data points. (Paper II)

The reason behind the difference in the response of wet foam to natural and re-generated fibres can be attributed to several factors: Fines reduce the surface tension, but they are too large and immobile to stabilise large bubble deformations. As shown in Fig. 4.14, the dynamic surface tension for a kraft fibre suspension decreases for long bubble life times. Regenerated fibres seem not to affect the dynamic surface tension at all since they are not associated with fines. Reduction of the dynamic surface tension in a kraft fibre suspension can explain the smaller average bubble size of Fig. 4.11b. On the other hand, rough surfaces can capture air and act as a reservoir for Ostwald ripening (Cantat et al. 2013). This can explain a larger proportion of middle-sized bubbles in Fig. 4.13.

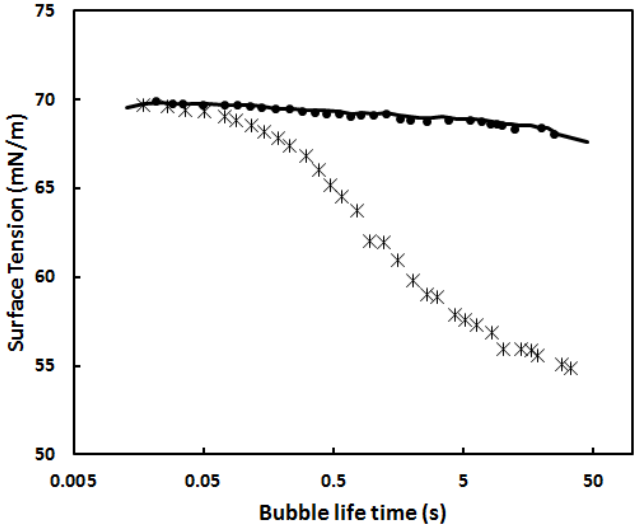

Figure 4.14. Dynamic surface tension for a varying bubble life time as measured with a BPA-800P bubble pressure tensiometer for a pure 0.2 g/l SDS (99% purity, solid curve), and the corresponding suspensions obtained by adding 0.33% refined kraft fibres (crosses) or rayon fibres (circles) to the stock. Rayon was used as a model regenerated fibre in the measurement because of its short length. (Paper II)

4.3 Fibre network structure

4.3.1 Foam- vs. water-forming

This section investigates the fibre network structure of paper manufactured using the foam-forming and water-forming technology. The basic sheet properties are given in Table 4.1. We fit the X-ray μCT pore size data with a linear combination of the Gaussian ($g(r)$) and log-normal distributions:

$$f(r) = A g(r, \mu_1, \sigma_1) + (1 - A)\,\mathrm{lognorm}(r, \mu_2, \sigma_2), \tag{4.1}$$

in which A is the (fitted) amplitude, $\mu_{1,2}$ and $\sigma_{1,2}$ are fitting parameters of the distributions, which describe the mean and standard deviation of $g(r)$ or similar parameters for the natural logarithm in the case of the log-normal distribution.

Figure 4.15 shows the volume-weighted pore size distributions of water-formed sheets obtained for CTMP and kraft fibres. It also shows the new fitting tion $f(r)$, log-normal and Gaussian distributions of both cases. It is evident that the characteristic shape of water-formed sheets for both types of fibres is dominated by the log-normal distribution. This is consistent with results of the previous studies (Bliwsner 1964; Niskanen 2008; Dodson and Sampson 1996). There is however a small contribution from the Gaussian component. This could be explained by many factors such as fibre flexibility, fibre orientation, forming consistency, hydrodynamic conditions during forming and fibre dimensions. All these factors play an important role on how fibres are distributed in a sheet. A slight deviation from the log-normal distribution is thus not surprising.

Table 4.1: Basic sheet properties of water-formed and foam-formed paper. In foam-forming, the surfactant concentrations were 0.2 g/l for the kraft pulp and 0.3 g/l for the CTMP pulp. (Paper III)

Fiber type	Rotation speed (RPM)	Grammage (g/m^2)	Thickness (µm)	Density (kg/m^3)
CTMP	2000	83.5	835.3±20.7	100.0±2.5
	3500	97.4	845.8±17.8	115.2±2.4
	5000	83.8	752.9±15.5	111.3±2.3
	6900	100.3	864.4±20.8	116.0±2.8
	Water	96.0	895.2±26.1	107.2±3.1
KRAFT	2000	98	559±17.6	175.3±5.5
	3500	110	557.3±20.1	197.4±7.1
	5000	104	536.6±17.9	193.8±6.5
	6900	112	520.6±18.1	215.1±7.5
	Water	101	420±21.2	240.5±12.1

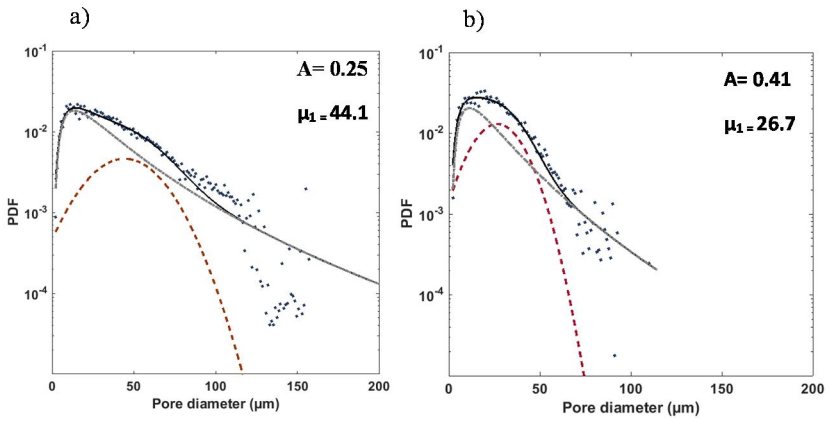

Figure 4.15. Volume-weighted pore size distributions (probability density functions PDF) of the water-formed sheets obtained for a) CTMP and b) kraft fibres. The solid lines are fits by Eq. (4.1) to the distribution whereas the dashed lines indicate the contributions to them of the log-normal and Gaussian components. A and μ_1 are parameters of the fitted Gaussian component, see Eq. (4.1). (Paper III)

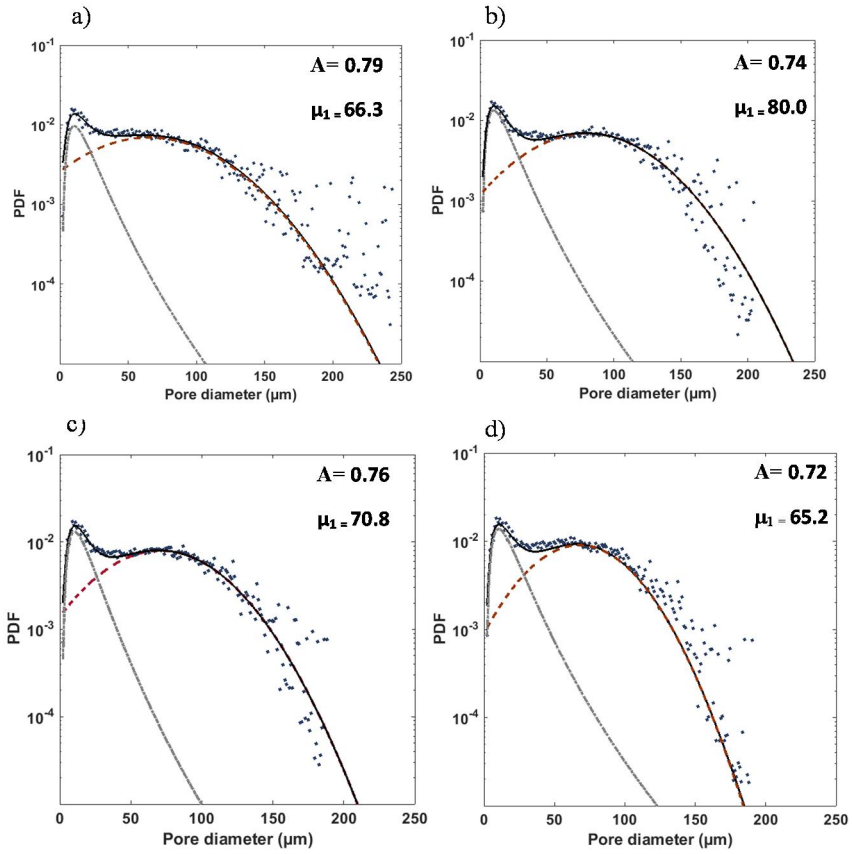

Figure 4.16. Volume-weighted pore size distributions of the foam-formed sheets obtained for CTMP fibres at rotation speeds a) 2000 RPM, b) 3500 RPM, c) 5000 RPM and d) 6900 RPM. The solid lines are fits by Eq. (4.1) to the distribution whereas the dashed lines indicate the contributions to it of the log-normal and Gaussian components. A and μ_1 are parameters of the fitted Gaussian component, see Eq. (4.1). (Paper III)

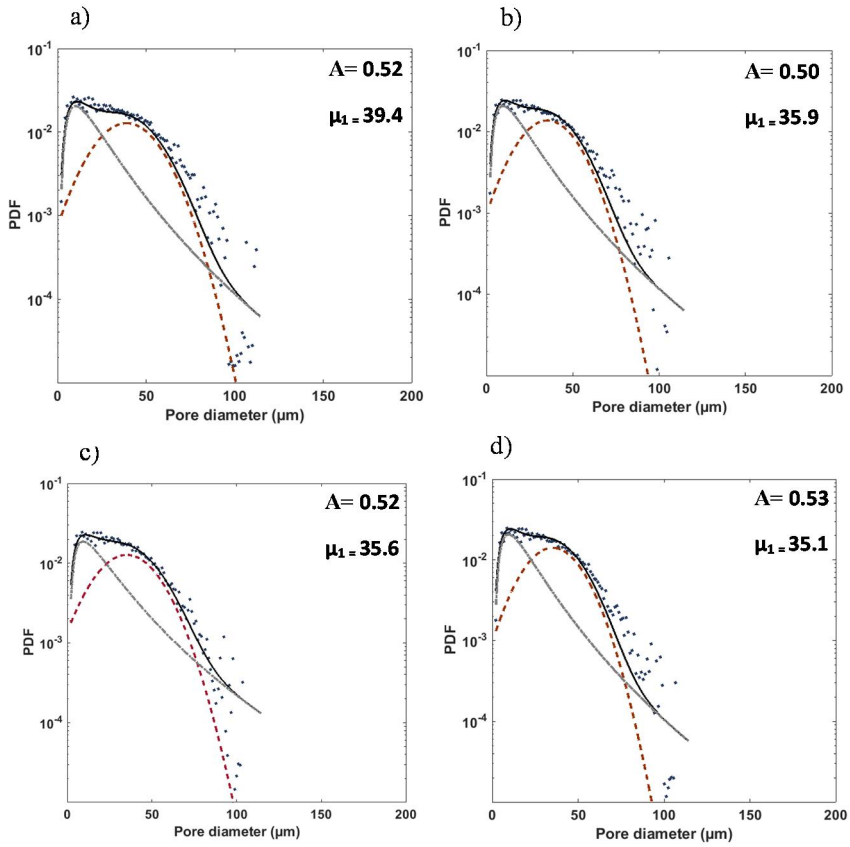

Figure 4.17. Volume-weighted pore size distributions of the foam-formed sheets obtained for kraft fibres at rotation speeds a) 2000 RPM, b) 3500 RPM, c) 5000 RPM and d) 6900 RPM. The solid lines are fits by Eq. (4.1) to the distribution whereas the dashed lines indicate the contributions to it by the log-normal and Gaussian components. A and μ_1 are parameters of the fitted Gaussian component, see Eq. (4.1). (Paper III)

Table 4.1: Parameters of the fitted pore size distributions (see Eq. (4.1)) for both foam-formed and water-formed paper made of CTMP and kraft fibres. A is the (fitted) Gaussian amplitude. $\mu_{1,2}$ and $\sigma_{1,2}$ are fitting parameters of the distributions, which describe the mean and standard deviation of the Gaussian distribution (index 1) or similar parameters for the natural logarithm in the case of the log-normal distribution (index 2). The last column gives the Sauter mean pore radius. (Paper III)

Fiber type	Medium	*A*	μ_1	σ_1	μ_2	σ_2	r_{32}
CTMP	Foam, 2000 RPM	0.79±0.03	66.3±3.3	43.9±1.8	2.9±0.1	0.67±0.06	63.7±1.3
	Foam, 3500 RPM	0.74±0.03	80.0±2.7	42.5±1.9	2.9±0.1	0.69±0.04	57.5±0.8
	Foam, 5000 RPM	0.76±0.03	70.8±2.1	38.0±1.5	2.9±0.1	0.65±0.04	51.9±0.7
	Foam, 6900 RPM	0.72±0.03	65.2±2.0	35.8±1.3	2.8±0.1	0.65±0.05	48.7±0.7
	Water	0.25±0.10	44.1±4.6	21.5±4.5	3.6±0.1	0.94±0.03	37.7±0.6
Kraft	Foam, 2000 RPM	0.52±0.18	39.4±3.0	18.0±2.5	3.0±0.2	0.83±0.10	26.5±0.6
	Foam, 3500 RPM	0.50±0.14	35.9±2.2	16.7±2.1	3.1±0.2	0.86±0.07	25.1±0.6
	Foam, 5000 RPM	0.52±0.15	35.6±2.2	16.6±2.1	3.1±0.2	0.86±0.08	24.9±0.6
	Foam, 6900 RPM	0.53±0.16	35.1±2.4	16.6±2.1	3.0±0.2	0.86±0.09	24.8±0.7
	Water	0.41±0.10	26.7±1.7	12.6±1.6	3.2±0.1	0.83±0.04	22.1±0.5

Figures 4.16 and 4.17 show the pore size distributions of foam-formed sheets made of CTMP and kraft fibres. The pore size distributions of the foam-formed sheets were much wider than those of the corresponding water-formed sheets. Equation 4.1 fits well the distributions of almost all foam-formed sheets. The characteristic shapes of the distributions of the foam-formed sheets are dominated by the Gaussian distributions. The fraction of the Gaussian distribution is larger for sheets made of the CTMP fibres for which parameter *A* was around 0.75, whereas its value was around 0.50 for sheets made of kraft fibres (Table 4.1).

The Gaussian component comes from interaction of fibres with bubbles. During the forming process, the air bubbles keep the fibres apart. This has an impact on the fibre orientation and also on fibre bending (see Fig. 4.18).

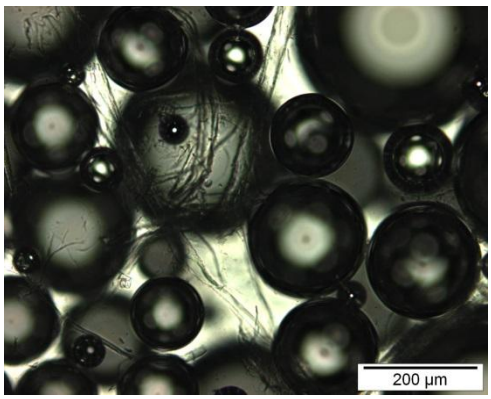

Figure 4.18. CTMP fibres (consistency 1.25%) in the foam made with SDS surfactant (concentration 1 g/l). The geometric restrictions caused by bubbles not only affect the location and orientation of fibres, but also cause their bending. (Paper III)

The pore size distributions of sheets made with foam-forming depends on foam properties. The relationship between the mean pore radius and the mean bubble radius of CTMP and kraft fibres are shown in Fig. 4.19, and in both cases the relationship is shown to be linear. It seems that in the case of stiff CTMP fibres the bubble size has a strong impact, stronger than in the case of flexible kraft fibres. We got almost the same values for the mean pore radii in sheets made by water-forming as extrapolation of the curve to vanishing or zero bubble size in sheets made with foam-forming.

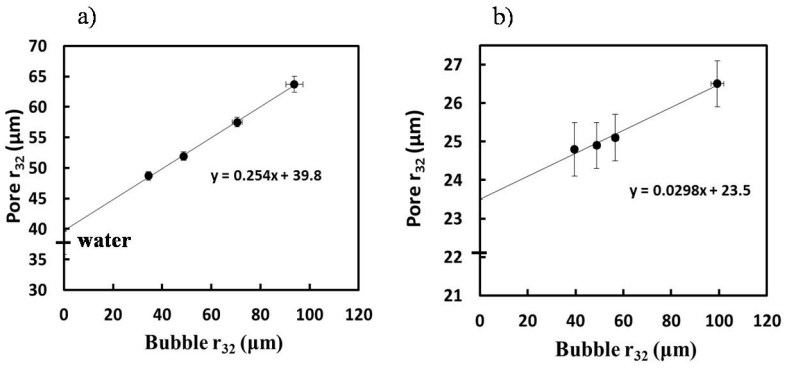

Figure 4.19. Sauter mean pore radius as a function of mean bubble radius for a) stiff CTMP fibres and b) flexible kraft fibres. The value of the mean pore radius for the water-formed sheets is shown in the y-axis. (Paper III)

4.3.2 Pore structure characterisation of foam-formed sheets using different imaging techniques

Because of recent developments in the foam-forming technology, need has emerged for an efficient characterisation of the porous structure at very low densities. In order to find an effective and practical choice among all structure characterisation methods imaging techniques were used to compare the pore size distribution of foam-formed samples made of two different types of cellulose fibre. The techniques included the X-ray micro-computed tomography (X-ray µCT), scanning electron microscopy (SEM), light microscopy (LM), and direct surface imaging using charge-coupled device (CCD) camera. The values obtained using X-ray µCT were used as a benchmark for other characterisation techniques since X-ray µCT allows scanning of the whole sample and gives more accurate information about pore structure analysis.

Figure 4.20 shows the mean pore radius for sheets obtained for CTMP and kraft fibres determined by X-ray µCT, SEM, LM and a CCD camera. Rotation speed of the mixer varied in the range 2000-6900 RPM. The 2-d methods slightly underestimated the mean pore size in the case of the CTMP sheets, and overestimated the pore size for the kraft sheets. Looking more closely at the pore size distributions, the 3-d approach indicated a smaller proportion of large pores even if the 3-d pores were volume-weighted and the 2-d pores area-weighted. Thus, it seems the voids differ strongly from a spherical shape.

For sheets made of CTMP fibres, there were clear differences in the results obtained by different characterisation techniques. The values obtained using SEM (cross-sectional) images were quite close to those obtained with X-ray µCT. Also, LM gave similar results at a low rotation speed. At high rotation speeds the values obtained using LM and a CCD camera images were quite similar with a significant difference from those obtained using X-ray µCT. On the other hand, comparison of the mean pore sizes as obtained by different methods from the sample made of kraft fibres showed to some extent a similar behaviour.

For SEM and LM, the number of images for each sample was four, which generally is not sufficient for pore size distributions of high accuracy. The foam-formed materials were however very homogeneous. The mean pore size could therefore be estimated quite accurately from only a few images.

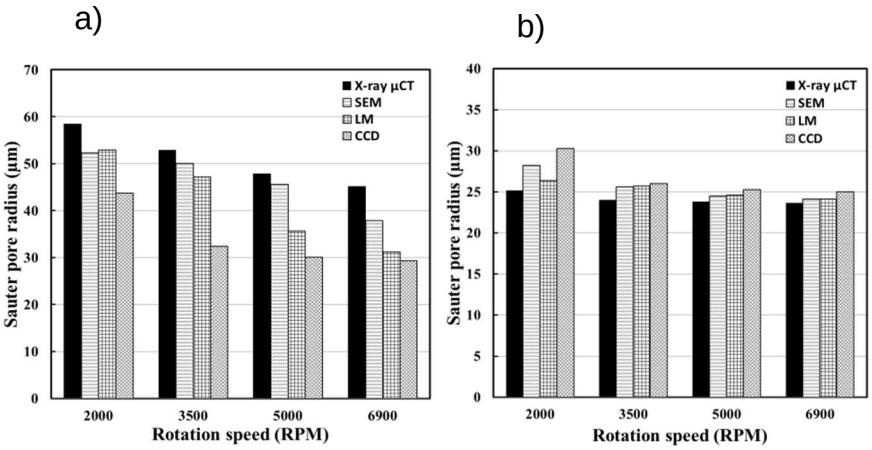

Figure 4.20. Sauter mean pore radius plotted against the rotation speed as determined by X-ray µCT, SEM, LM and CCD surface images for a) CTMP and b) Kraft sheets. (Paper IV)

4.3.3 Comparison of X-ray micro-computed tomography with mercury intrusion porosimetry

Figure 4.21 shows the total 3-d porosity of sheets made of kraft and CTMP fibres at respectively 2000 RPM and 6900 RPM as determined by X-ray CT and MIP. In general, the porosity of both furnishes shows quite similar results for the two techniques. The largest difference was found for the kraft sample made at 2000 RPM, its porosity was 0.83 and 0.91 respectively by X-ray µCT and MIP.

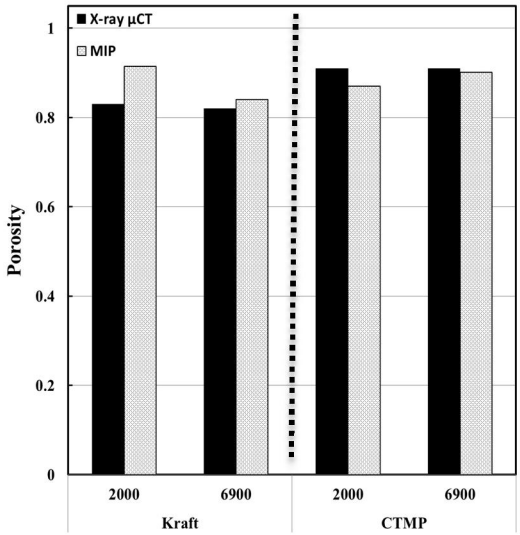

Figure 4.21. Porosity of foam-formed sheet samples made of kraft and CTMP fibres at 2000 RPM and 6900 RPM as determined by X-ray µCT and MIP. (Paper IV)

Figure 4.22 shows the mean pore radius determined by X-ray µCT and MIP of samples made of kraft and CTMP fibres at two rotation speeds, 2000 RPM and 6900 RPM. Overall, the mean pore radius as determined by MIP was higher for the kraft fibres. Situation was the opposite for the sheet made of the CTMP fibres at 2000 RPM. This can be explained by Fig. 4.23. Detection of pores larger than 115 µm is not possible with MIP. X-ray µCT can however determine pores bigger than this as there is no detection limit. The range of pore diameters in the sheet made of the CTMP fibres at 2000 RPM was 2-247 µm in the X-ray µCT -image and 0.0037-115 µm in the MIP-image, while at 6900 RPM they were respectively 2-170 µm and 0.0037-115 µm. In MIP pressure was increased incrementally, and because the CTMP sheet made at 2000 RPM was more porous than the one made at 6900 RPM, penetration of mercury was accomplished in a very short pressure range. Analysis was thus limited to small pores only (size below 115 µm).

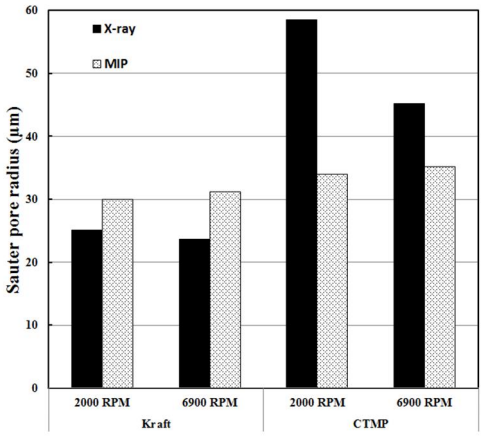

Figure 4.22. Mean pore radius of samples made of kraft and CTMP fibres at 2000 RPM and 6900 RPM, as obtained using X-ray µCT and MIP. (Paper IV)

In the medium pore-size range, the qualitative behaviour of the pore size distribution obtained by MIP for the CTMP fibres was similar to those obtained by X-ray µCT. MIP indicated an increased proposition of pores in the size range of the bubbles of the foam. This may be caused by the fast penetration paths along large pores formed by the foam-fibre interaction. Penetrating mercury may find these 'large-pore-routes' more easily than what is possible with structural imaging.

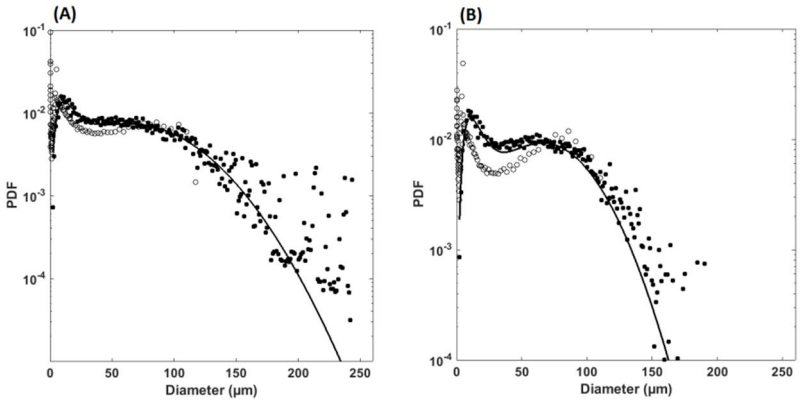

Figure 4.23. Volume-weighted pore size distributions (probability density functions, PDFs) of samples made of CTMP fibres as obtained by X-ray µCT (solid circles) and MIP (open circles) at rotation speeds A) 2000 RPM, and B) 6900 RPM. The solid curves represent fits of the X-ray µCT pore size data by a linear combination of the gaussian and log-normal distributions. (Paper IV)

4.4 Strength properties

It is important to understand the influence of sheet structure on its tensile properties. Density is a very important macroscopic structural parameter of paper and can be influenced by many factors such as fibre type, fibre consistency, wet pressing, drying process and many others. Accuracy of the determination of density is related to accuracy of the thickness measurements. As we pointed out earlier, thickness measurements were carried out with a device that largely avoided pressing the sheet during the measurement.

Figure 4.24 shows the apparent density of foam-formed and water-formed sheets. It is evident that the density of sheets made of the CTMP fibres is low in comparison with sheets made of the kraft fibres. In addition, the density of foam-formed kraft sheets varied with the rotation speed. This is not the case for the CTMP sheets however.

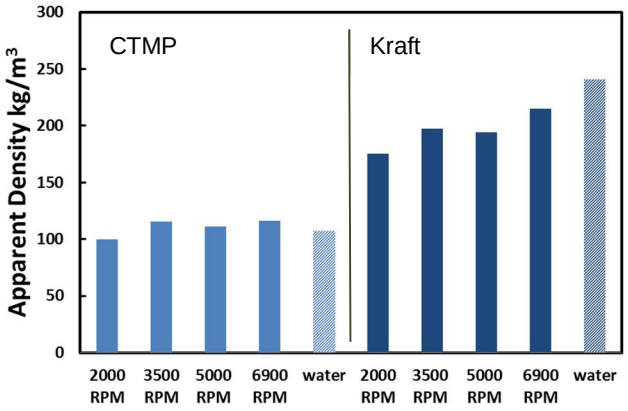

Figure 4.24. Apparent density of foam-formed sheets of a varying rotation speed and of water-formed sheets made of CTMP and kraft fibres. The CTMP sheets were made with an SDS concentration of 0.3 g/l, whereas kraft sheets were made with an SDS concentration of 0.2 g/l.

Measured values of the tensile strength of the kraft sheets correlated strongly with their measured density (Fig. 4.25). Situation was quite different for the CTMP sheets however. Their density varied much less with the rotation speed, and the corresponding water-formed and foam-formed sheets had a similar density with no apparent correlation with the rotation speed. The tensile strength of the sheets was however found to depend strongly on their mean pore size as shown in Fig. 4.26.

It is well known in the paper industry that there is a clear link between the bulk and strength properties of paper (Niskanen 2008).

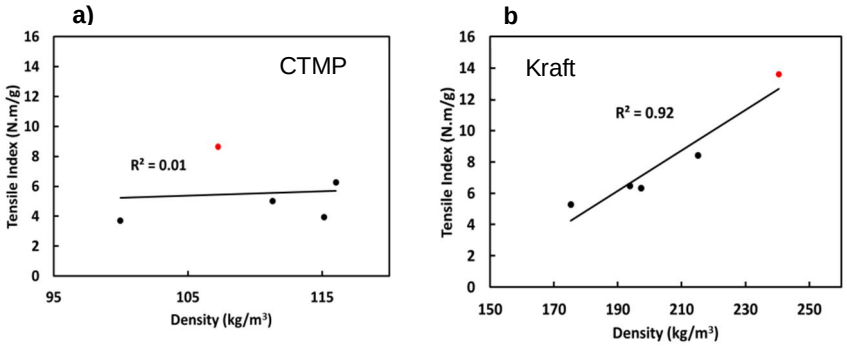

Figure 4.25. Tensile index in the machine direction plotted against density for a) CTMP and b) kraft fibres. Data include both foam-formed sheets for a varying rotation speed and water-formed sheets (red).

A narrower pore size distribution causes a more uniform microstructure of the network and a better connectedness of fibres. Moreover, in the foam-forming process, capillary forces become weaker during drainage, which could result in a reduced bonding of fibres.

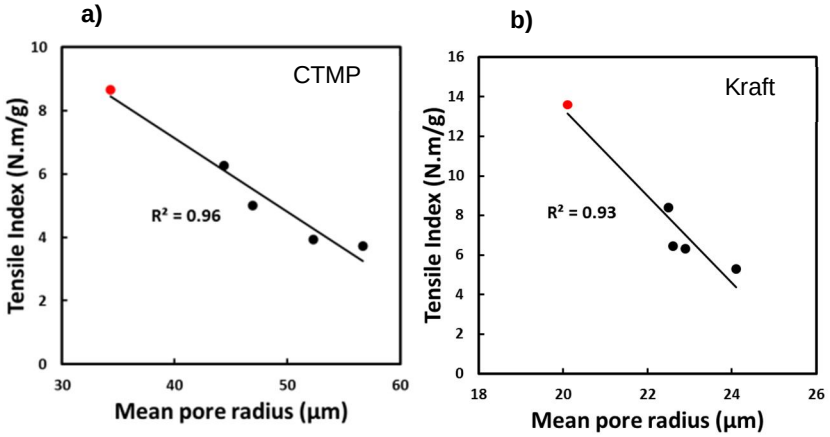

Figure 4.26. Tensile index in the machine direction plotted against the mean pore radius for a) CTMP and b) kraft fibres. Data include both foam-formed sheets for a varying rotation speed and water-formed sheets (red). (Paper III)

When comparing the tensile indices of kraft sheets made with 0.2 and 0.6 g/l SDS concentrations at a quite similar sheet density (Figs. 4.27 and 4.28), it appeared that adding more surfactant decreased the tensile strength. This difference was much larger in water-formed sheets however, where SDS had been added to the suspension without making foam. Moreover, in foam-forming the sheet density could be decreased more using a small quantity of SDS. This has a great practical importance in industrial processes.

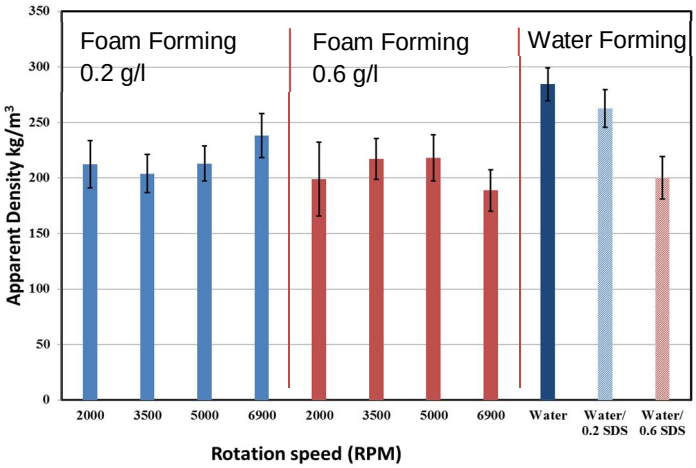

Figure 4.27: Apparent density of foam-formed sheets for a varying rotation speed and water-formed sheets of refined kraft fibres at 0.2 and 0.6 g/l SDS.

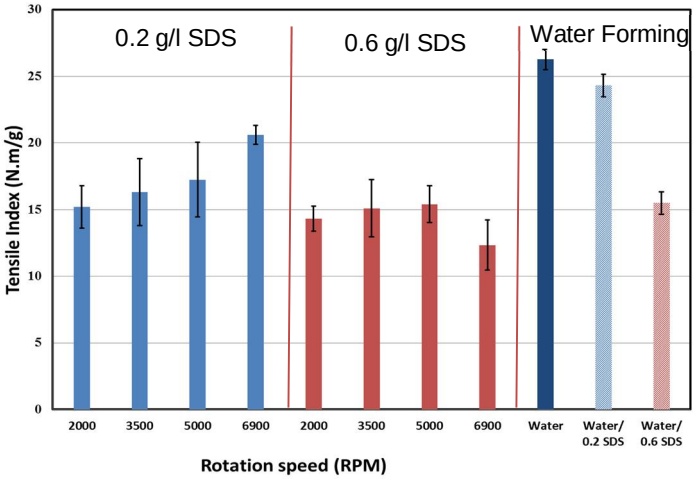

Figure 4.28. Tensile index of water-formed and foam-formed sheets of refined kraft fibres.

5. Conclusions

> Be sure that you go to the author to get at his meaning, not to find yours.
> —John Ruskin, Sesame and Lilies

Foams have been shown to produce novel fibre structures when used instead of water as the fibre carrier. This new forming technology produces materials of increased homogeneity, bulk and porosity with potential savings in raw materials, energy and water. Therefore, fundamental research is required on the main mechanisms underlying their material structure. The thesis discusses laboratory studies on basic foam-fibre interactions without complications caused by product-specific industrial processes like foam production, wet pressing, drying etc. All the objectives presented in Section 1.2 were met by the work. The main results and findings of this Thesis can be summarised in the following way:

Foam-fibre interaction: In axial mixing, the bubble size and its distribution could be affected by several factors such as the rotation speed, air content and surface tension. In axial mixing the mean bubble size could be described with a simple formula including air content as one of the parameters. Response of wet foam to natural and regenerated fibres was quite different. The mean bubble size became smaller for natural than regenerated fibres, and the bubble size distribution became narrower for natural fibres. The reasons behind this behaviour were likely to be the rough surfaces of the natural fibres and the related fraction of fine particles, which were absent for regenerated fibres. In the mixing of wet foam laden with fibres, fibre type influenced much the bubble size at a low or moderate mixing speed, whereas air content was insensitive to it. This has great practical importance, as quite often only air content is followed in industrial foam processes. At high rotation speeds however, beyond a macro-instability of the flow, also air content became sensitive to the type and consistency of the fibres.

Characterisation: The micro-structure of the sheets was characterised using X-ray micro-tomography, scanning electron microscopy, light microscopy, direct surface imaging using a CCD camera and mercury intrusion porosimetry. X-ray micro-tomography provided the best information about the porous structure. The 2-d microscopies (SEM, light microscopy) slightly underestimated the mean pore

size of samples with a significant amount of very large pores, and overestimated the pore size when the relative amount of small pores increased. The pore size distributions obtained from CCD camera images were surprisingly similar to those obtained by the other 2-d imaging techniques. It was possible in particular to observe changes in the pore structure caused by varying foam properties. Thus, this technique could have potential in an industrial control of the on-line quality for those uncoated products which do not require a significant wet pressing or contact drying during their production. Mercury intrusion porosimetry was able to characterise pore sizes also in the sub-micron region, but led to an increased relative volume of the pores around the mean bubble size of the foam. This may be related to the penetration channels created by the foam-fibre interaction.

Micro-structure: The microscopic pore structure of foam-formed sheets and water-formed sheets at a roughly equal density were significantly different. The pore size distribution of the foam-formed sheets was much wider than the corresponding distribution of the water-formed sheets. The characteristic shape of the distribution of foam-formed sheets was dominated by a Gaussian component, whereas in the water-formed sheets the distribution was dominated by a log-normal component. The pore size distribution of foam-formed sheets correlated with the mean bubble size. This had also an effect of tensile strength. In particular, for sheets with constant density, the tensile strength depended strongly on their mean pore size. In short, the foam-forming technology provides material with striking features such as improved bulk and porosity. Moreover, it is possible to tailor the formed structure with foam properties.

References

Aaltosalmi, U., Kataja, M., Koponen, A., Timonen, J., Goel, A., Lee, G. and Ramaswamy, S. 2004. Numerical analysis of fluid flow through fibrous porous materials, J. Pulp Paper Sci. 30, 251-255.

Alava, M., Niskanen, K. 2006. The physics of paper, Rep. Prog. Phys. 69, 669-723.

Bliesner, W.C. 1964. A study of the porous structure of fibrous sheets using permeability techniques, Tappi J. 47, 392-400.

Bock, J. and Jacobi, A.M. 2013. Geometric classification of open-cell metal foams using X-ray micro-computed tomography. Materials Characterization 75, 35–43.

Cantat, I., Cohen-Addad, S., Elias, F. Graner, F., Höhler, R., Pitois, O., Rouyer, F., and Saint-Jalmes, A. 2013. Foams: Structure and dynamics. Oxford University Press, Oxford, 265 p.

Chatterjee, A., Moulik, S.P., Sanyal, S.K., Mishra, B.K., Puri, P.M. 2001. Thermodynamics of micelle formation of ionic surfactants: A critical assessment for sodium dodecyl sulphate, cetyl pyridinium chloride and dioctyl sulfosuccinate (Na salt) by microcalorimetric, conductometric and tensiometric measurements. J. Phys. Chem. B 105, 12823-12831.

Chinga, G. 2002. Structural studies of LWC paper coating layers using SEM and image analysis techniques, Norwegian university of science and technology, Norway, 108.

Chinga-Carrasco, G. 2009. Exploring the multi-scale structure of printing paper – a review of modern technology, Journal of Microscopy, 234, 211–242.

Chinga-Carrasco, G., Maria, A., Øyvind, E., Stina, S. 2008. Structural characteristics of pore networks affecting print-through, Journal of Pulp and Paper Science (JPPS), ISSN, 34 (1), 13-22.

Clark, N.O. 1948. The electrical conductivity of foam. Transactions of the Faraday Society 44,13–15.

Clift, R., Grace, J. R., Weber, M. E. 1978. Bubbles, drops, and particles, Academic press, INC, New York.

Darton, R. C.; Sun, K.-H. 1999. The effect of surfactant on foam and froth properties. Trans. IChemE, 77, 535-542.

Darton, R., Sun, K. 1999. The effect of surfactant on foam and froth properties, Trans. IChemE 77, 535-542.

Denkov, N.D., Tcholakova, S., Golemanov, K. Ananthpadmanabhan, K.P, Lips, A. 2009. The role of surfactant type and bubble surface mobility in foam rheology, Soft Matter 5, 3389-3408.

Dodson C.T.J., and Sampson, W.W. 1996. The effect of paper formation and grammage on its pore size distribution. J. Pulp Pap. Sci. 22, 165-169.

Edited by Ek, M., Gellerstedt, G., Henriksson, G. 2009. Paper Products Physics and Technology, Walter de Gruyter GmbH & Co. KG, 10785 Berlin. 335.

Exerowa, D., Kruglyakov, P. M. 1998. Foam and foam films: Theory, experiment, application. Elsevier Science B. V., Amsterdam. 773.

Gane, P., Cathy, R., Esa, L., Rustem, V. 2004. Comparison of NMR Cryoporometry, Mercury Intrusion Porosimetry, and DSC Thermoporosimetry in Characterizing Pore Size Distributions of Compressed Finely Ground Calcium Carbonate Structures, Ind. Eng. Chem. Res., 43, 7920–7927.

Gardiner, B., Dlugogorski, B., Jameson, G. 1999. Prediction of pressure losses in pipe flow of aqueous foams, Ind. Eng. Chem. Res. 38,1099–1106.

Gatward, A.P.J. 1973. Long-fibres developments in the UK and Europe, Giving at a meeting of London division, Paper Technology.

Goel, A., Tzanakakis, M., Huang, S., Ramaswamy, S., Choi D. and Ramarao, B.V. 2001. Characterization of the three-dimensional structure of paper using X-ray microtomography, Tappi J. 84, 72-80.

Gonzenbach, U.T, Studart, A.R., Tervoort, E., Gauckler, L.J., 2007. Tailoring the microstructure of particle-stabilized wet foams, Langmuir 23, 1025-1032.

Gonzenbach, U.T., Studart, A.R., Tervoort, E., Gauckler, L.G. 2006. Stabilization of foams with inorganic colloidal particles. Langmuir 22, 10983–10988.

Hasal, P., Jahoda, M., Fořt, I. 2008. Macro-instability: a chaotic flow component in stirred tanks, Phil. Trans. R. Soc. A 366, 409-418.

Hildebrand T. and Rüesgsegger, P. 1996. A new method for the model-independent assessment of thickness in three-dimensional images, J. of Microscopy, 185, 67-75.

Hinze, J. O. 1955. Fundamentals of the hydrodynamic mechanism of splitting in dispersion processes. AIChE J. 1, 289-295.

Hjelt, T., Kinnunen, K., Lehmonen, J., Beletski, N., Hellén, E., Liljeström, V., Serimaa, R., Miettinen, A., Kataja, M. 2011. Intriguing structural and strength behavior in foam forming, Progress in Paper Physics Seminar, Graz, 135.

Hohler, R., Cohen-Addad, S. 2005. Rheology of liquid foam, J. Phys.: Condens. Matter 17, R1041–R1069.

Holmstad, R. 2004. Methods for paper structure characterisation by means of image analysis, Norwegian university of science and technology, Norway, 211.

Industrial Computed Tomography Systems. www.xviewct.com.

Isarin, J.C., Kaasjager A.D.J., and Holweg R.B.M. 1985. Bubble size distribution during the application of foam to fabrics and its effects on product quality. Textile Res. J. 65(2), 61-69.

Jäsberg, A., Selenius, P., Koponen, A. 2015. Experimental results on the flow rheology of fiber-laden aqueous foams. Colloids and Surfaces A: Physicochem. Eng. Aspects 473, 147-155.

Kidner, T. 1974. The Radfoam Process for Fine Papers. Paper Technology, 15 (6), 346-351.

Kinnunen K., Lehmonen J. Beletski N., Jetsu P. and Hjelt T. 2013. Benefits of foam forming technology and its applicability in high MFC addition structures. The 15th Pulp and Paper Fundamental Research Symposium, 8-13 September, Cambridge. pp 837-850.

Kroezen, A. B. J.; Groot Wassink, J. 1987. Bubble size distribution and energy dissipation in foam mixers. JSDC, 103, 386-394.

Lappalainen, T., Lehmonen, J. 2012. Determinations of bubble size distribution of foam-fibre mixture using circular hough transform, Nordic Pulp Paper Res. J. 27, 930-939.

Lappalainen, T., Salminen, K., Kinnunen, K., Järvinen, M., Mira, I., Andersson, M. 2014. Foam Forming Revisited. Part II. Effect of surfactant on the properties of foam-formed paper products, Nordic Pulp Paper Res. J. 29, 689–699.

Larmignat, S., Vanderpool, D., Lai, H.K., Pilon, L. 2008. Rheology of colloidal gas aphrons (microfoams), Colloids Surf. A: Physicochem. Eng. Aspects 322, 199–210.

Lehmonen, J., Jetsu, P., Kinnunen, K., Hjelt, T. 2013. Potential of foam-laid forming technology for paper applications, Nordic Pulp Paper Res. J. 28, 392-398.

Malysa K, Lunkenheimer K. 2008. Foams under dynamic conditions. Curr Opin Colloid Interface Sci, 13:150.

Metzner, A.B., Otto, R.E. 1957. Agitation of non-Newtonian fluids, AIChE J. 3, 3-11.

Mira, I., Andersson, M., Boge, L., Blute, I., Carlsson, G., Salminen, K., Lappalainen, T., Kinnunen, K., 2014. Foam Forming Revisited. Part I. Foaming behaviour of fibre-surfactant systems, Nordic Pulp Paper Res. J.

Moura, M.J., Ferreira, P.J., Figueiredo, M.M. 2005. Mercury intrusion porosimetry in pulp and paper technology technology, Powder Technology, 160, 61-66.

Nazarzadeh, E.; Sajjadi, S. 2010. Viscosity effects in miniemulsification via ultrasound. AIChE J. 56, 2751-2755.

Niskanen K., 2008 (ed.). Paper Physics. 2nd edition, Paperi ja Puu Oy, Helsinki. 360.

Nordic forest owners' association. http://www.nordicforestry.org/facts/finland.asp.

Nouri, J., Whitelaw, J. 1990. Flow characteristics of stirred reactors with Newtonian and non-Newtonian fluids, AIChE J. 36, 627-629.

Paper and board − Determination of grammage − , ISO 536: 1995.

Paper and board − Determination of opacity (paper backing) − Diffuse reflectance method, ISO 2471:2008.

Paper and board − Determination of roughness/smoothness (air leak methods) − Part 2: Bendtsen method, ISO 8791-2: 1990.

Paper and board − Determination of tensile properties − Part 2: Constant rate of elongation method, ISO 1924-2: 1994.

Poranen, J. 2012. Resource Efficiency with Foam Forming. FIBIC's EffFibre & Effnet Seminar. Nov. 22, 2012. http://fibic.fi/other/efffibre-effnet-seminar-presentations

Poranen, J., Kiiskinen, H., Salmela, J., Asikainen, J., Keränen, J., Paakkonen, E. 2013. Breakthrough in papermaking resource efficiency with foam forming. Proceedings of TAPPI PaperCon 2013, vol. 1, Atlanta, GA, USA. P. 807–814.

Pugh RJ. 1996. Foaming, foam films, antifoaming and defoaming. Adv Colloid Interf Sci, 64:67.

Punton V.W. 1975. The use of an aqueous foam as a fibre-suspending medium in quality papermaking. In Akers R.J., ed. Foams. Proceedings of a symposium organized by the Society of chemical industry. Colloid and surface chemistry Group, Brunel University. September 8-10.

Radvan, B., Gatward, A.P.J. 1972. The Formation of Wet-Laid Webs by a Foaming Process, Tappi 55, 748.

Rodriques R.T., and Rubio J. 2003. New basis for measuring the size distribution of bubbles. Miner. Eng. 16, 757-765.

Rosen, M. J. 2004. Surfactant and Interfacial Phenomena. John Wiley & Sons Inc, Hoboken, New Jersey, 444 .

Rosenfeld, A. and Pfaltz, J.L. 1966. Sequential operations in digital picture processing, J. Assos. Comput. Mach., 13(4), pp. 471-494.

Saint-Jalmes, A. Physical chemistry in foam drainage and coarsening. *Soft Matter* **2006**, 2, 836-849.

Saito T. and Toriwaki, J. 1994. New algorithms for Euclidean distance transformation on an n-dimensional digitized picture with applications, Pattern Recognition 27, 1551-1565.

Samuelsen, E.J., Gregersen, O.W., Houen, P.J., Helle, T., Raven, C., Snigirev, A. 2001. Three-dimensional imaging of paper by use of synchrotron X-ray microtomography, J. Pulp Paper Sci. 27, 50-53.

Sievänen, H. 2010. Suitability of foam coating on application of thin liquid films, Master's Thesis, Lappeenranta University of Technology.

Skelton, J. 1987. Foam assisted dewatering – a new technology emerges. Paper Technology, 28, 431-436.

Smith, M.K., Punton, V.W., Rixson, A.G. 1974. The structure and properties of paper formed by a foaming process, Tappi 57, 107-111.

Tcholakova, S., Denkov, N.D, Golemanov, K., Ananthapadmanabhan, K.P., Lips, A. 2008. Theoretical model of viscous friction inside steadily sheared foams and concentrated emulsions, Phys. Rev. E 78, 011405.

Ventura-Medina, E., Cilliers, J.J., 2000. Calculation of the speci7c surface area in flotation. Minerals Engineering 13 (3), 265–275.

Vernhes, P., Rolland du Roscoat, S., Blayo, A., Pineaux, B., Thibault, X., Bloch, J.-F. 2008. Synchrotron X-ray Microtomography: A New Tool to Characterize the Interaction Between Paper and Toner, Journal of Imaging Science and Technology 52(1): 010502–010506.

Wang, Y.; Neethling, S. J. 2009. The relationship between the surface and internal structure of dry foam. Colloids and Surfaces A: Physicochem. Eng. Aspects, 339, 73-81.

Weaire, D., and Hutzler, W. 1999.The Physics of Foams, Clarendon Press. Oxford, 1-55.

Xie, W., Neethling, S.J., Cilliers, J.J. 2004. Anovel approach for estimating the average bubble size for foams &owing in vertical columns, Chemical Engineering Science 59, 81 – 86.

Appendix A: Corrigendum

The author regrets that there is a typing error in Equation 17 in Paper I. The correct equation should be without a number 4 in the denominator.